Heliyon 9 (2023) e17642

Contents lists available at ScienceDirect

Heliyon

journal homepage: www.cell.com/heliyon

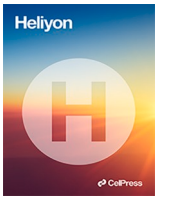

A fractional model of magnetohydrodynamics Oldroyd-B fluid with couple stresses, heat and mass transfer: A comparison among Non-Newtonian fluid models

Muhammad Arif [a,b], Poom Kumam [a,b,c], Thidaporn Seangwattana [d,*], Panawan Suttiarporn [d]

[a] *Fixed Point Research Laboratory, Fixed Point Theory and Applications Research Group, Center of Excellence in Theoretical and Computational Science (TaCS-CoE), Faculty of Science, King Mongkut's University of Technology Thonburi (KMUTT), 126 Pracha Uthit Rd., Bang Mod, Thung Khru, Bangkok, 10140, Thailand*

[b] *Center of Excellence in Theoretical and Computational Science (TaCS-CoE), Faculty of Science, King Mongkut's University of Technology Thonburi (KMUTT), 126 Pracha Uthit Rd., Bang Mod, Thung Khru, Bangkok, 10140, Thailand*

[c] *Department of Medical Research, China Medical University Hospital, China Medical University, Taichung, 40402, Taiwan*

[d] *Faculty of Science Energy and Environment, King Mongkut's University of Technology North Bangkok, Rayong Campus (KMUTNB), 21120, Rayong, Thailand*

ARTICLE INFO

Keywords:
Oldroyd-B couple stress fluid (OBCSF)
Atangana-baleanu fractional derivatives
Magnetohydrodynamics
Porous media
Channel flow

ABSTRACT

The present article aims to extend some of the already existing fluid models to a large class of fluids namely, "Oldroyd-B couple stress fluid (OBCSF)". The main focus of the present work is to combine the existing fluid models in ordered to get a new class of fluid. The unsteady magnetohydrodynamics (MHD) Oldroyd-B fluid (OBF) with couple stresses, porosity, heat and mass transfer is considered in the present analysis. The Oldroyd-B couple stress fluid is assumed to flow in channel. The classical model is fractionalized by considering Atangana-Baleanu (AB) operator in ordered to highlight the memory analysis. To develop closed form solutions the combined (Laplace + Fourier) integrals have been used. The results obtained are portrayed through graphs for all pertinent flow parameters which involved in the present dynamic model. Moreover, the impact of AB time fractional parameter is investigated graphically on flow, temperature and concentration distributions exploiting MATHCAD software. Secondly, for better understanding the present solutions of Oldroyd-B couple stress fluid (OBCSF) are reduced to Odroyd-B fluid (OBF) without couple stresses, Maxwell solutions, Couple stress solutions and Newtonian viscous fluid solutions and the results have been compared for classical and fractional order derivatives. In addition to this a limiting case is carried out by our solutions to already published work which verify our solutions. In addition to this during the analysis we noticed that the flow heat and concentrated get lowered for the escalating numerical values of AB fractional derivatives. Similarly, it is also noticed that the velocity in channel accelerated with the increment of numeric values of pressure, porosity, thermal buoyancy and relaxation time parameter. In the same manner temperature and concertation profiles gets low with the higher values of Prandtl number, Reynold number and fractional operator. Finally, skin friction for momentum equation, Nusselt number for temperature and Sherwood number for concentration have been calculated and given in tabular forms.

* Corresponding author.
E-mail address: thidaporn.s@sciee.kmutnb.ac.th (T. Seangwattana).

https://doi.org/10.1016/j.heliyon.2023.e17642
Received 19 October 2022; Received in revised form 24 May 2023; Accepted 23 June 2023
Available online 3 July 2023

1. Introduction

The researchers are taking interest in the flows of non-Newtonian fluids due to world-wide use and its practical uses in various fields of engineering and sciences. There are many types of non-Newtonian fluids like, grease, oil, drugs, lubricants, plastic, honey, cool tar, paint and toothpaste etc. And these fluids are described by different non-Newtonian fluid models. Simple Navier-Stokes equations cannot describe these non-Newtonian fluid models. In order to explain the characteristics, features and the dynamics there exists many models which describe non-Newtonian fluids.

The Oldroyd-B fluid model is a constitutive equation used to describe the behavior of viscoelastic fluids, which exhibit both viscous and elastic properties. The model was introduced by Oldroyd [1] in 1950 and is commonly used in the study of polymer solutions, melts, and other complex fluids. The Oldroyd-B model assumes that the stress tensor in the fluid can be decomposed into two parts: a purely viscous contribution and a contribution due to the deformation of elastic molecules within the fluid. The elastic contribution is described using a generalized Maxwell model, which consists of a series of springs and dashpots in parallel. The resulting constitutive equation is a partial differential equation relating the stress tensor to the rate of deformation tensor.

Furthermore, in the Oldroyd-B model where the author derived a non-Newtonian fluid model namely "Oldroyd-B fluid". It is the type of non-Newtonian fluid model which store energy as a linear elastic solid material and the dissipation of this model is due to the dissipative mechanism and rise from the mixture of two viscous fluids. The fluid have this kind of properties can be describe as stress relaxation time, creep and the difference between the normal shear stresses which developed during simple shear flows. This special fluid have the property to use as for describing the response of polymeric liquids. The nature of OBF is same like non-Newtonian fluid because the stress and rate of strain have non-linear relationship. Further OBF classified and has the characteristics of rate type fluid. Oldroyd was the first who developed the method for the flow of rate type fluid. OBF has many enormous practical uses in fluid dynamics. It is worth noting that the OBF is the generalized version of viscoelastic Maxwell model [2]. Motivated from the applications of OBF in real life an increasing number of researchers have been attracted to perform their studies by considering this advance class of the fluid. Recently, many researchers studied the characteristics and flow behavior of OBF in different circumstances, like Prema et al. [3] where the author studied OBF and explain the heat and mass transfer within the porous medium. Hamza et al. [4] developed the flow of MHD OBF in porous medium along with the external pressure. Fetecau et al. [5] collected some characteristics of OBF and wrote a note on the flows of OBF by choosing the plate having constant acceleration. In another paper Fetecau et al. [6] concerning the efficiency of the unsteady OBF by taking the impulsive motion of the plate between the two side walls which are perpendicular to the plate. Elhanafy et al. [7] calculated the solutions of this complex model by employing the numerical scheme and discussed the applications of hemodynamics. Tahir et al. [8] discussing the impact of OBF flow passing through the two rotating cylinders. Mahmud et al. [9] investigated the impact of magnetic field and the influence of shear thinning with zero mass flux by assuming the applications of Oldroyd-B fluid model. In another paper Mahmud et al. [10] studied Oldroyd-B fluid with the impact of chemical reaction MHD effect and the flow is a non-Fourier heat flux model with physical applications.

The non-Newtonian fluids have useful applications when dealing with real world problems and due to this reason, the non-Newtonian fluids getting more attention of the researchers from the last few decades. Then scientists and mathematicians like, Euler, Newton, Navier, Stokes, Abel and Fourier etc, constructed many fluid models to analyze the dynamics of non-Newtonian fluid in nature and developed different equations to describe the characteristic behavior of the fluid flow models. To highlight the flow behavior of Couple stress fluid (CSF) model which is one of the non-Newtonian fluid model. This idea is given by famous mathematician Stokes in 1964 [11] who introduce the CSF. CSF model is the generalized form of simple Navier-Stokes theory. The CSF model has the polar effect like, the body couples and couple stresses are considered to develop the fluid flow. The equation of motion for CSF is quiet similar to Navier-Stokes theory with an extra term of order four. The CSF model explain many fluid flow like, liquid crystals, muddy water, greases, engine oil, honey and animal blood [12]. There are many studies recorded to explain the uses of CSF theory. Let us recall some of the studies like, Arif et al. [13] where the author investigated CSF flow in between channel along with the pressure exerted on the fluid externally, and for solutions using the applications of integral transforms, Laplace and Fourier. Similarly, some unique solutions can be found in the study of Reddy et al. [14] who developed the CSF fluid model and provided some advance applications of CSF with the impact of MHD heat and mass transfer in the radiative flow of vertical cylinder. Recently, some interesting results of CSF have been highlighted by the authors in various physical situations like, Kumar et al. [15] where the authors inspected CSF fluid using the method of differential transform to the unsteady free convection flow over stretching sheet. Some other aspects of CSF fluid with the super critical heat transfer analysis of the flow due to a vertical cylinder with applications is inspected by Basha et al. [16]. Moreover, Herimath et al. [17] and Reddy et al. [18] developed CSF model and calculated the numerical investigations in the heat and mass transfer phenomena under the influence of moving cylinder and shrinking porous sheet. Mehmood et al. [19] explained the effects of thermal diffusion on the flow of couple stress fluid over a stretched plate with the applications of high order chemical reaction.

In the last few decades, the depicted scenarios, an increasing real-life applications of fractional order derivatives which is widely used in heterogeneous set of fluid dynamics as well as the memory effect in different dynamical systems. There are many complex dynamical systems which cannot be highlighted by applying the derivatives. Therefore, it is worth mentioning that the involvement of fractional order derivatives is used to highlight some of the hidden properties of different dynamical systems which is known as sensitive memory effect. The FC played a vital role in every field of sciences like, engineering, biological sciences and industrial sciences. From the last few decades visualizes that fractional derivative is more appropriate as compared to simple derivatives due to its unique memory property. Fractional calculus become a vast field due to its enormous applications in modern science. Therefore, a variety of fractional operators have been introduced and use in different situations. In all operator the most famous operator which is

developed by Atangana-Baleanu (AB) [20] in 2016. They modified the CF operator and developed a fractional operator have non-singular and non-local kernel. This AB fractional derivatives have many applications in the field of fluid dynamics and industrial sciences. Let us recall some recently developed fractional models and their applications to fluid dynamics. Recently, Arif et al. [21] where the authors discussed the influence and dynamics of CSF in channel with the involvement of external pressure, it is worth mentioning in this study that the fractional results obtained for Caputo-Fabrizio (CF) and Atangana-Baleanu (AB) fractional derivatives have been compared and highlight in graphs. Similarly, work have been done by Arif et al. [22], where the author have considered the impact of fractional derivatives on the Casson fluid with ramped wall temperature. In addition, Baleanu and Agarwal [23] highlighted some advance applications of fractional calculus the details is given in a very famous article which name as "Fractional Calculus in the Sky". In another paper Baleanu [24], where the author concerning the evaluation of the memory effect of fractional derivatives in different real-world problems. In addition to this Bas and Ozarslan [25] analyzed some real-world applications of AB fractional derivatives in modern sciences and technology. Similarly, Syam and Al-Refai [26] added some advance applications of AB fractional derivatives. Addition to this AB operator describe the hidden sensitive properties of a dynamical system with a good memory and explained the sensitivity analysis of the physical models. The models developed by taking AB operator can be describe many complex physical situations with an appropriate result. Furthermore, the term "memory" means to highlight the hidden sensitive properties of any physical phenomena that's why fractional derivative has been used.

The research of heat and mass transfer have various physical applications in different thermal and cooling systems. It is the reason that the scholars take interest in the phenomena of heat and mass transfer and highlighted their useful applications. Heat and mass transfer phenomenon use in different physical situations, industries, heat pumps, turbines, heat generator, and many other fields of sciences and engineering. Motivated from the modern applications of heat and mass transfer some fundamental applications are presented in the book of Bergman et al. [27]. In the paper of Arif et al. [28] where the author explained the presence of heat and mass transfer in working fluids using nanoparticles for the thermal transport properties, with the impact of ramped heating. Similarly, the comprehensive information regarding to heat and mass transfer for practicing engineers and researchers are given in the book of Kothandaraman [29] where the author discussed the advance thermal characteristics of heat and mass transfer. In another paper, Khan et al. [30] studied the phenomena of heat and mass transfer of the fluid which are allowed to pass through shrinking permeable surfaces.

The electrically conducting fluid with magnetohydrodynamics (MHD) flow in channel have enormous applications, like MHD generator, magnetic therapy, MRI, MHD turbines and some applications in engineering and sciences. Let us to give some relevant examples in Fabich [31] where the author examined MHD applications using the high power protons beam shocks in a mercury jet target for neutrino factory. In another paper, Asadullah et al. [32] developed MHD Jeffery fluid flow for the advance applications in fluid dynamics and discussed the fluid flow in channel. Furthermore, the applications of MHD is given by Ali et al. [33] where the authors discussed the impact of MHD on Casson fluid with the influence of heat, thermal radiation and chemical reaction on the fluid flow. Similarly, Zheng et al. [34] studied MHD effect in non-Newtonian Oldroyd-B fluid flow fluid is disturbed and start motion due to the accelerating plate employing the fractional operator and the exact solutions have been recovered using the Fox H-function with the discrete Laplace transform. In addition to this some unique features of Oldroyd-B fluid with MHD effect have been highlighted by Abbasi et al. [35]. Furthermore, in another paper Sravanthi et al. [36] and Abbasi et al. [37] where the authors inspected the impact of the Oldroyd-B fluid with MHD effect by highlighting various physical applications. Furthermore, some new advance and unique applications of MHD in fluid flow problems have been investigated by Rashid et al. [38] where the authors inspected EMHD nanofluid in curved channel through corrugated walls. Riaz et al. [39] describe some new insight into the cilia motion through electrically conducting fluid with MHD applications. Some other advance applications of MHD in various real-life applications is given in Refs. [40–42].

The main novelty of the present research work is to extend available results from the literature to a new class of fluid namely, "Oldroyd-B couple stress fluid". This is for the first time the two non-Newtonian fluid models collected and developed in this analysis as a new model and given a name as "Oldroyd-B couple stress fluid model". In the literature this model is developed for the first time which is not calculated before that is the reason to consider it and fill the gap, which is the main novelty of the present analysis. Motivated from the above the flow of incompressible unsteady MHD Oldroyd-B couple stress fluid has been considered in order to highlight its impact on the heat and mass transport phenomena. Furthermore, in the study the famous Atangana-Baleanu time fractional derivative is applied to generalize the Oldroyd-B couple stress fluid model for describing the sensitive memory effects in the fluid dynamics. Additionally, the present work established the exact solutions of the Oldroyd-B couple stress fluid model of order four using the joint applications of the Laplace and finite Fourier sine transforms. We provide the exact solutions of the corresponding momentum, energy and concentration equations. Moreover, the skin friction, Nusselt number and Sherwood number are presented in tabular form. The influence of all parameters is investigated which affect the fluid flow. Furthermore, the influence of AB time fractional parameter is highlighted on flow, temperature and concentration distributions. Secondly, for better understanding the present solutions are reduced to Maxwell solutions, Odroyd-B solutions without couple stresses, Couple stress solutions and Newtonian viscous fluid solutions and compared these solutions for classical and fractional order derivatives. Apart from several other applications the present work is significance and worthwhile as the exact solutions obtained during this study are important and not only new, but these exact solutions can be used as bench mark for numerical solvers and it will helped them to verify different numerical schemes. Finally, the rest of the paper is arranged as follow. The mathematical modeling of the present work is given in section 2. Section 3 aims to formulate the given model. The present classical model is transformed by applying the Atangana-Baleanu fractional model is provided in section 4. Furthermore, the solutions of energy, concentration and momentum equation is provided in subsection 4.1, 4.2 and 4.3 respectively. Some special cases of the given model are provided in section 5. The Nusselt number, Sherwood number and skin friction are given in section 6. The graphical results and discussion is presented in section 7. The conclusion of the present analysis is

provided in section 8. At the end of the manuscript the appendix have been provided.

The present analysis we have considered the following assumptions.

- We have considered the impact of couple stresses in the Oldroyd-B fluid make them and advance class of non-Newtonian fluid model have many applications
- The present study describes heat and mass transfer effect of the fluid flow.
- The fluid is considered in the channel with external pressure.
- The classical model have been transformed by considering the AB fractional derivatives.
- The present analysis the impact of MHD and porosity are also considered.

2. Mathematical modeling

The OBF with CSF effect have been considered in this report. The incompressible unsteady flow of OBCSF is taken in channel. In addition this research addressed the impact of MHD and porosity with the collective thermal and concentration effect. The fluid is allowed in channel bounded by plates with distance d between them. The fluid is taken in porous channel with the involvement of external pressure and also the magnetic field B_0 is taken which is normal to the fluid motion. The governing equations of the flow are given by Ref. [43]:

The continuity equation must satisfied because we have considered the incompressible fluid.

$$\nabla \cdot \vec{\mathbf{V}} = 0, \tag{1}$$

The vector notation of momentum equation is given by Ref. [43]:

$$\rho\left[\frac{\partial \vec{V}}{\partial t} + \left(\vec{V}\cdot\nabla\right)\vec{V}\right] = -\nabla p + \mathrm{div}\mathbf{T} - \eta\nabla\times\left(\nabla\times\left(\nabla\times\left(\nabla\times\vec{\mathbf{V}}\right)\right)\right) + \mathbf{J}\times\mathbf{B} + g\rho\beta(T-T_\infty) + g\rho\beta(C-C_\infty) + \Re. \tag{2}$$

The expression for heat equation is as follows:

$$\rho c_p \frac{\partial \vec{\mathbf{T}}}{\partial t} = k\nabla\times\nabla\times\vec{\mathbf{T}}, \tag{3}$$

The mass equations mathematically can be expressed as:

$$\frac{\partial \vec{\mathbf{C}}}{\partial t} = D\nabla\times\nabla\times\vec{\mathbf{C}}, \tag{4}$$

where $\vec{\mathbf{V}}, \vec{\mathbf{T}}$ and $\vec{\mathbf{C}}$ are the vector form of velocity, temperature and concentration. Where $\rho, \boldsymbol{J}, \boldsymbol{B}, g, \eta, \beta_T, \beta_C\, k, D, c_p, \Re$, and t represents density of the fluid, current density of the fluid, MHD, gravity, couple stress parameter, volume thermal expansion, volume concentration expansion, thermal conductivity, diffusivity, specific heat, Darcy's resistance and time of the fluid respectively. Furthermore, vector form of velocity $\vec{\mathrm{V}}$ temeprature $\vec{\mathbf{T}}$, concentration $\vec{\mathbf{C}}$ and Cauchy stress tensor $\mathbf{T}$ for OBF for unidirectional and one dimension can be defined as:

The velocity flow, energy and concentration component form can be expressed as:

$$\vec{\mathbf{V}} = (u(y,t),0,0), \vec{\mathbf{T}} = (T(y,t),0,0) \quad \text{and} \quad \vec{\mathbf{C}} = (C(y,t),0,0). \tag{5}$$

From the expressions defined above it is clear that the flow heat and concertation of the present study is along the x-axis.

Mathematically representation of Cauchy stress is given below [44,45]:

$$\mathbf{T} = \mathbf{S} - p\mathbf{I}\,. \tag{6}$$

Where $\mathbf{S}$ and $-p\mathbf{I}$ here shows the extra stress and indeterminate stresses respectively. Additionally, $\mathbf{S}$ can be defined as:

$$\mu\left(1+\frac{\lambda_1.\mathbf{D}}{\mathbf{D}\mathrm{t}}\right) = \mathbf{S}\left(1+\frac{\lambda_2.\mathbf{D}}{\mathbf{D}\mathrm{t}}\right), \tag{7}$$

In the above expression μ, λ_1 and λ_2 shows dynamic viscosity, retardation time and relaxation time respectively. Furthermore, material time derivative $\frac{\mathbf{D}}{\mathbf{D}\mathrm{t}}$ and Rivilin-Ericksen tensor $\mathbf{A}_1$ can be written as:

$$\frac{\mathbf{DS}}{\mathbf{D}\mathrm{t}} = \frac{\partial \mathbf{S}}{\partial t} + u\left(\frac{\partial \mathbf{S}}{\partial x}\right) + v\left(\frac{\partial \mathbf{S}}{\partial y}\right) + w\left(\frac{\partial \mathbf{S}}{\partial z}\right), \tag{8}$$

$$\mathbf{A}_1 = \nabla.\vec{V} + \left(\nabla.\vec{V}\right)^T = \begin{bmatrix} 0 & u_y \\ u_y & 0 \end{bmatrix}. \tag{9}$$

In the given study we have consider OBF, therefor, there is a modification in Darcy's law.
[1, 46]:

$$-\frac{\mu\varphi}{k_0}\left(1+\lambda_{\Re}\frac{\partial}{\partial t}\right).\overrightarrow{V}=\left(1+\lambda\frac{\partial}{\partial t}\right)\Re, \tag{10}$$

In the above law φ and k notations for porous medium and the porous medium permeability. Maxwell equation can be expressed as:

$$\overrightarrow{\nabla}\cdot\boldsymbol{B}=0, \tag{11}$$

$$\overrightarrow{\nabla}\times\overrightarrow{E}=-\frac{\partial\boldsymbol{B}}{\partial E}=0, \text{ where we have total electric field } E=0, \tag{12}$$

The total electric field is represented by E and by Ohm's Law (the generalized form) can be expressed as:

$$\boldsymbol{J}=\sigma\left(\overrightarrow{E}+\overrightarrow{V}\times\boldsymbol{B}\right)=\sigma\left(\overrightarrow{V}\times\boldsymbol{B}\right). \tag{13}$$

From above we get:

$$\boldsymbol{J}\times\boldsymbol{B}=\sigma\left(\overrightarrow{V}\times\boldsymbol{B}\right)\times\boldsymbol{B}\,\boldsymbol{B}=B_0+b, \tag{14}$$

The above MHD term can be expressed in more suitable form as:

$$\boldsymbol{J}\times\boldsymbol{B}=-\sigma\left\{\boldsymbol{B}\times\left(\overrightarrow{V}\times\boldsymbol{B}\right)\right\}=-\sigma\left\{(\boldsymbol{B}\cdot\boldsymbol{B})\overrightarrow{V}-\left(\boldsymbol{B}\cdot\overrightarrow{V}\right)\boldsymbol{B}\right\}, \tag{15}$$

$$\boldsymbol{J}\times\boldsymbol{B}=-\sigma\left\{(\boldsymbol{B}\cdot\boldsymbol{B})\overrightarrow{V}-0\right\}=-\sigma\boldsymbol{B}_0^2u. \tag{16}$$

Using equations 5–16, applying Maxwell equation and Darcy's law and multiply it by $\left(1+\lambda\frac{\partial}{\partial t}\right)$ Eq. (2) becomes:

$$\begin{aligned}\rho\left(1+\lambda\frac{\partial}{\partial t}\right)\frac{\partial u}{\partial t}&=G+\mu\left(1+\lambda_{\Re}\frac{\partial}{\partial t}\right)\frac{\partial^2u}{\partial y^2}-\eta_0\left(1+\lambda\frac{\partial}{\partial t}\right)\frac{\partial^4u}{\partial y^4}-\sigma\boldsymbol{B}_0^2\left(1+\lambda\frac{\partial}{\partial t}\right)u\\&-\frac{\mu\varphi}{k_0}\left(1+\lambda_{\Re}\frac{\partial}{\partial t}\right)u+g\rho\beta\left(1+\lambda\frac{\partial}{\partial t}\right)(T-T_\infty)+g\rho\beta\left(1+\lambda\frac{\partial}{\partial t}\right)(C-C_\infty).\end{aligned} \tag{17}$$

Equation (17) represents the momentum equation of the present flow.

3. Formulation of the problem

This research is focused on the new class of fluid model known as "Oldroyd-B couple stress fluid (OBCSF)" flow in channel. The OBCSF passing through the porous channel with the impact of MHD and external pressure. The fluid is assumed to flow in a vertical channel and initially both the left and right plate were at rest having ambient temperature T_∞ and concertation C_∞. After some times the left plate start motion with a constant velocity and the temperature and concertation at the left plate raised to the surface temperature T and concertation C. The geometrical representation of the considered model is given in Fig. 1.

The system of equations which describe the given flow model is given in Eqs. 18–20 along with the IC's and BC's which is provided in Eq. (21) ref. [1,46,47]:

$$\begin{aligned}\rho\left(1+\lambda\frac{\partial}{\partial t}\right)\frac{\partial u}{\partial t}&=G+\mu\left(1+\lambda_{\Re}\frac{\partial}{\partial t}\right)\frac{\partial^2u}{\partial y^2}-\eta_0\left(1+\lambda\frac{\partial}{\partial t}\right)\frac{\partial^4u}{\partial y^4}-\sigma\boldsymbol{B}_0^2\left(1+\lambda\frac{\partial}{\partial t}\right)u\\&-\frac{\mu\varphi}{k_0}\left(1+\lambda_{\Re}\frac{\partial}{\partial t}\right)u+g\rho\beta\left(1+\lambda\frac{\partial}{\partial t}\right)(T-T_\infty)+g\rho\beta\left(1+\lambda\frac{\partial}{\partial t}\right)(C-C_\infty),\end{aligned} \tag{18}$$

$$\left(\rho c_p\right)\frac{\partial T(y,t)}{\partial t}=k\frac{\partial^2T(y,t)}{\partial y^2}, \tag{19}$$

$$\frac{\partial C(y,t)}{\partial t}=D\frac{\partial^2C(y,t)}{\partial y^2}, \tag{20}$$

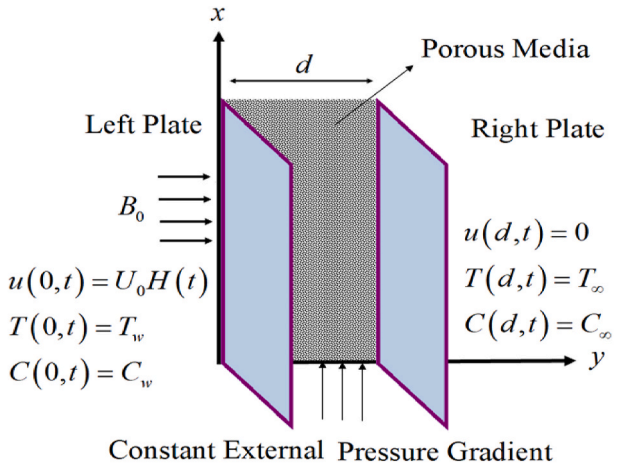

(a)

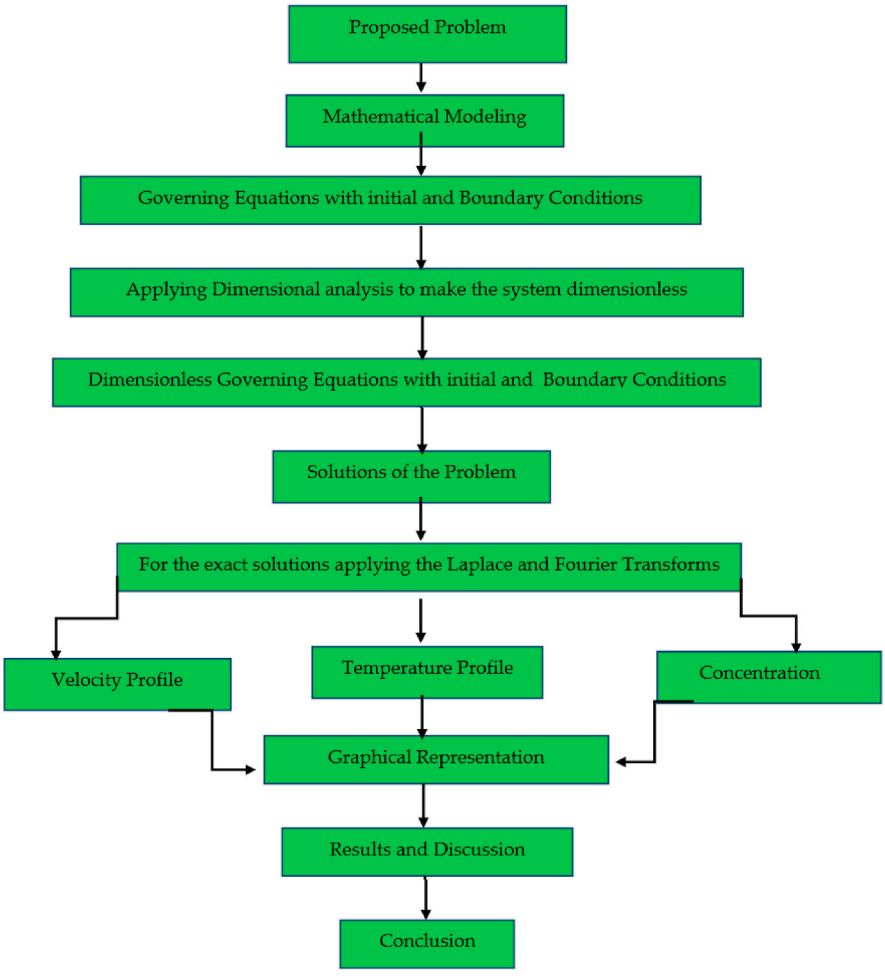

(b)

(caption on next page)

Fig. 1. (A): Geometry of the problem.
Fig. 1 (b): Solution Methodology and operational framework.

$$\left.\begin{array}{l}\left.\begin{array}{l}u(y,t)=0\\T(y,t)=T_\infty\\C(y,t)=C_\infty\end{array}\right\}\text{for},0<y<d\ \text{ and }\ t=0,\\\left.\begin{array}{l}u(y,t)=H(t)U_0\\T(y,t)=T_w\\C(y,t)=C_w\end{array}\right\}\text{for},y=0\ \text{ and }\ t>0,\\\left.\begin{array}{l}u(d,t)=0\\T(d,t)=T\\C(d,t)=C_\infty\\\dfrac{\partial^2u(0,t)}{\partial y^2}=\dfrac{\partial^2u(d,t)}{\partial y^2}=0\end{array}\right\}\text{for},y=0,y=d\ \text{ and }\ t>0.\end{array}\right\}. \tag{21}$$

To make the governing equations along with IC's and BC's dimensionless the following variables are used which is given in (22):

$$\xi=\frac{y}{d},\mathrm{w}=\frac{u}{U_0},\tau=\frac{U_0t}{d},\eta=\frac{\eta_0}{\mu d^2},P=\frac{d^2}{\mu U_0}G,\Theta=\frac{T-T_\infty}{T_w-T_\infty},\Phi=\frac{C-C_\infty}{C_w-C_\infty},\Big\}. \tag{22}$$

The dimensionless system of equations are:

$$\begin{aligned}&\mathrm{Re}\left(1+\lambda_1\frac{\partial}{\partial\tau}\right)\frac{\partial w(\xi,\tau)}{\partial\tau}=P+\left(1+\lambda_2\frac{\partial}{\partial\tau}\right)\frac{\partial^2w(\xi,\tau)}{\partial\xi^2}\\&-\eta\left(1+\lambda_1\frac{\partial}{\partial\tau}\right)\frac{\partial^4w(\xi,\tau)}{\partial\xi^4}-M\left(1+\lambda_1\frac{\partial}{\partial\tau}\right)w(\xi,\tau)\\&-\frac{1}{K}\left(1+\lambda_2\frac{\partial}{\partial\tau}\right)w(\xi,\tau)+Gr\left(1+\lambda_1\frac{\partial}{\partial\tau}\right)\Theta(\xi,\tau)+Gm\left(1+\lambda_1\frac{\partial}{\partial\tau}\right)\Phi(\xi,\tau),\end{aligned} \tag{23}$$

$$b_1\frac{\partial\Theta(\xi,\tau)}{\partial\tau}=\frac{\partial^2\Theta(\xi,\tau)}{\partial\xi^2}, \tag{24}$$

$$b_2\frac{\partial\Phi(\xi,\tau)}{\partial\tau}=\frac{\partial^2\Phi(\xi,\tau)}{\partial\xi^2}, \tag{25}$$

$$\left.\begin{array}{l}w(\xi,0)=0,\Theta(\xi,0)=0,\Phi(\xi,0)=0,\text{for}\ 0\le\xi\le1\\w(0,\tau)=1,\Theta(0,\tau)=1,\Phi(0,\tau)=1,\text{for}\ \tau>0,\\w(1,\tau)=0,\Theta(1,\tau)=0,\Phi(1,\tau)=0,\text{for}\ \tau>0,\\\dfrac{\partial^2w(0,\tau)}{\partial\xi^2}=\dfrac{\partial^2w(1,\tau)}{\partial\xi^2}=0,\text{for}\ \tau>0,\end{array}\right\}. \tag{26}$$

Where

$$Gr=\frac{g\rho\beta_T d^2(T_w-T_\infty)}{U_0\mu},Gm=\frac{g\rho\beta_C d^2(C_w-C_\infty)}{U_0\mu},\mathrm{Pr}=\frac{\mu c_p}{k},\mathrm{Re}=\frac{U_0d}{\upsilon},Sc=\frac{\upsilon}{D},$$

$$M=\frac{\sigma\boldsymbol{B}_0^2d^2}{\mu},\frac{1}{K}=\frac{d^2\varphi}{k_0},\lambda_1=\frac{\lambda U_0^2}{\upsilon},\lambda_2=\frac{\lambda_\Re U_0^2}{\upsilon},b_1=\mathrm{Pr.Re},b_2=Sc..\mathrm{Re}.$$

Where Gr and Gm represents Grashof and modified Grashof number, Pr and Re represent Prandtl and Reynolds number, similarly, Sc, M and K represents Schmidth number, magnetic parameter and porous media parameter respectively, λ_1 and λ_2 relaxation and retardation parameter respectively.

Definition: The AB fractional derivative of fractional order β is defined as [20].

$$ {}^{AB}\wp_{\tau}^{\beta}(\tau)=\frac{Z(\beta)}{(1-\beta)}\int_{0}^{\tau}E_{\beta}\left(\frac{-\beta(\tau-t)^{\beta}}{1-\beta}\right)f'(\tau)dt, \tag{27}$$

where $Z(\beta)$ is normalization function such that $Z(1)=Z(0)=1$ and $\beta\in(0,1)$..

Where from Eq. (27) E_{β} is the generalized Mittag-Leffler function [48].

$$ E_{\beta}\left(-t^{\beta}\right)=\sum_{k=0}^{\infty}\frac{(-t)^{\beta k}}{\Gamma(\beta k+1)}. \tag{28}$$

The LT of AB is given below:

$$ L\left({}^{AB}\wp_{\tau}^{\beta}(\tau)\right)=\frac{s^{\beta}L(\eta(\tau))-s^{\beta-1}\eta(0)}{(1-\beta)s^{\beta}+\beta}. \tag{29}$$

The generalized Mittag-Leffler function is provided in Eq. (28) and The LT of AB definition is given in Eq. (29).

4. Atangana-Baleanu fractional model

Applying the AB time fractional derivative, equations 23–25 can be written in generalized form as:

$$\begin{aligned}\mathrm{Re}\left(1+\lambda_1{}^{AB}\wp_{\tau}^{\beta}\right){}^{AB}\wp_{\tau}^{\beta}w(\xi,\tau)&=P+\left(1+\lambda_2{}^{AB}\wp_{\tau}^{\beta}\right)\frac{\partial^2 w(\xi,\tau)}{\partial\xi^2}-\eta\left(1+\lambda_1{}^{AB}\wp_{\tau}^{\beta}\right)\frac{\partial^4 w(\xi,\tau)}{\partial\xi^4}\\&-M\left(1+\lambda_1{}^{AB}\wp_{\tau}^{\beta}\right)w(\xi,\tau)-\frac{1}{K}\left(1+\lambda_2{}^{AB}\wp_{\tau}^{\beta}\right)w(\xi,\tau)+Gr\left(1+\lambda_1{}^{AB}\wp_{\tau}^{\beta}\right)\Theta(\xi,\tau)\\&+Gm\left(1+\lambda_1{}^{AB}\wp_{\tau}^{\beta}\right)\Phi(\xi,\tau),\end{aligned} \tag{30}$$

$$ b_1{}^{AB}\wp_{\tau}^{\beta}\Theta(\xi,\tau)=\frac{\partial^2\Theta(\xi,\tau)}{\partial\xi^2}, \tag{31}$$

$$ b_2{}^{AB}\wp_{\tau}^{\beta}\Phi(\xi,\tau)=\frac{\partial^2\Phi(\xi,\tau)}{\partial\xi^2}\ . \tag{32}$$

The generalized system of equations is given in Eqs. 30–32

4.1. Exact solutions of energy equation

The proposed model can be evaluated by using the Laplace transform to equation (31) and imposing the given conditions from equation (26) we get the transform results as:

$$ b_1.\frac{q^{\beta}}{(1-\beta)q^{\beta}+\beta}\overline{\Theta}(\xi,q)=\frac{d^2\overline{\Theta}(\xi,q)}{d\xi^2}, \tag{33}$$

equation (33) can be written in more convenient form as given in Eq. (34):

$$ \frac{m_0.q^{\beta}}{q^{\beta}+m_1}\overline{\Theta}(\xi,q)=\frac{d^2\overline{\Theta}(\xi,q)}{d\xi^2}, \tag{34}$$

With the Fourier finite sine transform that read as given in Eq. (35):

$$ \frac{m_0.q^{\beta}}{q^{\beta}+m_1}\overline{\Theta}_{Ns}(N,q)=-\gamma_N\overline{\Theta}_{Ns}(N,q)+\gamma_N\overline{\Theta}(0,q), \tag{35}$$

equivalently, we can write as:

$$ \overline{\Theta}_{Ns}(N,q)=\frac{m_2(q^{\beta}+m_1)}{q(q^{\beta}+m_3)}, \tag{36}$$

applying partial fraction on Eq. (36) we get:

$$ \overline{\Theta}_{Ns}(N,q)=\frac{m_1.m_2}{m_3.q}+\frac{m_2(m_3-m_1)}{m_3}\frac{1}{q^{1-\beta}(q^{\beta}+m_3)}, \tag{37}$$

by applying inverse LT, Equation (37) becomes:

$$ \Theta_{Ns}(N,\tau)=\frac{m_1.m_2}{m_3}+\frac{m_2(m_3-m_1)}{m_3}h(\tau)*F_{\beta}(-m_3,\tau), \tag{38}$$

Equation (38), represents the solution after applying Laplace inverse transform.

Applying the inverse Fourier transform we get:

$$\Theta(\xi,\tau)=1-\frac{\xi}{d}-\left(\frac{\xi(d-1)}{d}\right)+\frac{2}{d}\sum_{N=1}^{\infty}\frac{m_2(m_3-m_1)}{m_3}h(\tau)*F_\beta(-m_3,\tau)\sin\left(\frac{N\pi\xi}{d}\right). \tag{39}$$

Equation (39), shows the final solutions of the energy equation.

4.2. Exact solutions of concentration equation

For the exact solutions first applying the Laplace transform to concentration equation (32) and imposing the IC's from equation (26), we get:

$$b_2.\frac{q^\beta}{(1-\beta)q^\beta+\beta}\overline{\Phi}(\xi,q)=\frac{d^2\overline{\Phi}(\xi,q)}{d\xi^2}, \tag{40}$$

equation (40) can be written as:

$$\frac{m_4.q^\beta}{q^\beta+m_1}\overline{\Phi}(\xi,q)=\frac{d^2\overline{\Phi}(\xi,q)}{d\xi^2}, \tag{41}$$

applying the Fourier finite sine transform to Eq. (41) the results obtaining:

$$\frac{m_4.q^\beta}{q^\beta+m_1}\overline{\Phi}_{Ns}(N,q)=-\gamma_N\overline{\Phi}_{Ns}(N,q)+\gamma_N\overline{\Phi}(0,q), \tag{42}$$

Simplifying Eq. (42), we get the following result:

$$\overline{\Phi}_{Ns}(N,q)=\frac{m_5(q^\beta+m_1)}{q(q^\beta+m_6)}, \tag{43}$$

applying partial fraction on Eq. (43), we get:

$$\overline{\Phi}_{Ns}(N,q)=\frac{m_5.m_1}{m_6.q}+\frac{m_5(m_6-m_1)}{m_6}\frac{1}{q^{1-\beta}(q^\beta+m_6)}, \tag{44}$$

by applying inverse LT, Equation (44) becomes:

$$\Phi_{Ns}(N,\tau)=\frac{m_5.m_1}{m_6}+\frac{m_5(m_6-m_1)}{m_6}h(\tau)*F_\beta(-m_6,\tau), \tag{45}$$

applying the inverse Fourier transform on Eq. (45), we get:

$$\Phi(\xi,\tau)=1-\frac{\xi}{d}-\left(\frac{\xi(d-1)}{d}\right)+\frac{2}{d}\sum_{N=1}^{\infty}\frac{m_5(m_6-m_1)}{m_6}h(\tau)*F_\beta(-m_4,\tau)\sin\left(\frac{N\pi\xi}{d}\right). \tag{46}$$

Equation (46) shows the final solution of the concentration equation.

4.3. Exact solutions of momentum equation

For the exact solutions of momentum, the Laplace transform is applied to equation (30) and using conditions from equation (26), we get:

$$\begin{aligned}\mathrm{Re}\left(1+\lambda_1\frac{q^\beta}{(1-\beta)q^\beta+\beta}\right)\frac{q^\beta}{(1-\beta)q^\beta+\beta}\overline{w}(\xi,q)&=\frac{P}{q}+\left(1+\lambda_2\frac{q^\beta}{(1-\beta)q^\beta+\beta}\right)\frac{\partial^2\overline{w}(\xi,q)}{\partial\xi^2}\\&-\eta\left(1+\lambda_1\frac{q^\beta}{(1-\beta)q^\beta+\beta}\right)\frac{\partial^4\overline{w}(\xi,q)}{\partial\xi^4}-M\left(1+\lambda_1\frac{q^\beta}{(1-\beta)q^\beta+\beta}\right)\overline{w}(\xi,q)\\&-\frac{1}{K}\left(1+\lambda_2\frac{q^\beta}{(1-\beta)q^\beta+\beta}\right)\overline{w}(\xi,q)+Gr\overline{\Theta}(\xi,q)+Gm\overline{\Phi}(\xi,q),\end{aligned} \tag{47}$$

equation (47) becomes:

$$\begin{aligned}\mathrm{Re}\left(1+\lambda_1\frac{m_7.q^\beta}{q^\beta+m_1}\right)\frac{m_7.q^\beta}{q^\beta+m_1}\overline{w}(\xi,q)&=\frac{P}{q}+\left(1+\lambda_2\frac{m_7.q^\beta}{q^\beta+m_1}\right)\frac{\partial^2\overline{w}(\xi,q)}{\partial\xi^2}\\&-\eta\left(1+\lambda_1\frac{m_7.q^\beta}{q^\beta+m_1}\right)\frac{\partial^4\overline{w}(\xi,q)}{\partial\xi^4}-M\left(1+\lambda_1\frac{m_7.q^\beta}{q^\beta+m_1}\right)\overline{w}(\xi,q)\\&-\frac{1}{K}\left(1+\lambda_2\frac{m_7.q^\beta}{q^\beta+m_1}\right)\overline{w}(\xi,q)+Gr\overline{\Theta}(\xi,q)+Gm\overline{\Phi}(\xi,q),\end{aligned} \tag{48}$$

applying the Fourier finite sine transform to Eq. (48), we get:

$$\begin{aligned}\mathrm{Re}\left(1+\lambda_1\frac{m_7.q^\beta}{q^\beta+m_1}\right)\frac{m_7.q^\beta}{q^\beta+m_1}\overline{w}_{Ns}(N,q)&=\frac{P}{q}+\left(1+\lambda_2\frac{m_7.q^\beta}{q^\beta+m_1}\right)\left[-\gamma_N^2\overline{w}_{Ns}(N,q)+\gamma_N\overline{w}(0,q)\right]\\&-\eta\left(1+\lambda_1\frac{m_7.q^\beta}{q^\beta+m_1}\right)\left[\gamma_N^4\overline{w}_{Ns}(N,q)-\gamma_N^3\overline{w}(0,q)\right]-M\left(1+\lambda_1\frac{m_7.q^\beta}{q^\beta+m_1}\right)\overline{w}_{Ns}(N,q)\\&-\frac{1}{K}\left(1+\lambda_2\frac{m_7.q^\beta}{q^\beta+m_1}\right)\overline{w}_{Ns}(N,q)+Gr\overline{\Theta}_{Ns}(N,q)+Gm\overline{\Phi}_{Ns}(N,q),\end{aligned}\tag{49}$$

after some calculi Eq. (49), can be written as given below:

$$\begin{aligned}\overline{w}_{Ns}(N,q)&=\left[\frac{q^\beta+m_1}{m_{18}\left(q^\beta+m_{10}\right)\left(q^\beta+m_{15}\right)+m_{19}\left(q^\beta+m_{12}\right)\left(q^\beta+m_1\right)}\right]\times\frac{m_{16}\left(q^\beta+m_{17}\right)}{q}\\&\left[\frac{\left(q^\beta+m_1\right)^2}{m_{18}\left(q^\beta+m_{10}\right)\left(q^\beta+m_{15}\right)+m_{19}\left(q^\beta+m_{12}\right)\left(q^\beta+m_1\right)}\right]\times Gr\overline{\Theta}_{Ns}(N,q)\\&\left[\frac{\left(q^\beta+m_1\right)^2}{m_{18}\left(q^\beta+m_{10}\right)\left(q^\beta+m_{15}\right)+m_{19}\left(q^\beta+m_{12}\right)\left(q^\beta+m_1\right)}\right]\times Gm\overline{\Phi}_{Ns}(N,q),\end{aligned}\tag{50}$$

The result in Eq. (50) obtained after applying the Laplace and Fourier transforms.

$$\begin{aligned}\overline{w}_{Ns}(N,q)&=\frac{m_{16}\left(q^{2\beta}+m_{20}q^\beta+m_{21}\right)}{q\left(m_{22}q^{2\beta}+m_{23}q^\beta+m_{24}\right)}\\&\left[\frac{\left(q^\beta+m_1\right)^2}{q\left(m_{22}q^{2\beta}+m_{23}q^\beta+m_{24}\right)}\right]\times\left[Gr\overline{\Theta}_{Ns}(N,q)+Gm\overline{\Phi}_{Ns}(N,q)\right],\end{aligned}\tag{51}$$

Equation (51), can be expressed in more simplified form as:

$$\overline{w}_{Ns}(N,q)=A(q)+B(q)\times\left[Gr\overline{\Theta}_{Ns}(N,q)+Gm\overline{\Phi}_{Ns}(N,q)\right],\tag{52}$$

applying Laplace inverse on Eq. (52), we get the following result:

$$w_{Ns}(N,\tau)=A(\tau)+B(\tau)^*\left[Gr\Theta_{Ns}(N,\tau)+Gm\Phi_{Ns}(N,\tau)\right],\tag{53}$$

now applying the Fourier inverse on Eq. (53), we get the following result:

$$w(\xi,\tau)=\frac{2}{d}\sum_{N=1}^{\infty}(A(\tau))\sin\left(\frac{N\pi\xi}{h}\right)+\frac{2}{d}\sum_{N=1}^{\infty}\left[B(\tau)^*\left[Gr\Theta(\xi,\tau)+Gm\Phi(\xi,\tau)\right]\right]\sin\left(\frac{N\pi\xi}{h}\right).\tag{54}$$

Equation (54), present the final solutions of the momentum equation.

5. Special cases

5.1. Solution of Oldroyd-B fluid velocity

By putting the couple stress parameter = 0 , our solutions of velocity profile reduced to simple oldroyd-B fluid without couple stresses. To find the solutions repeating the above-mentioned process we get the solutions of Oldroyd-B fluid without couple stresses.

$$\begin{aligned}\mathrm{Re}\left(1+\lambda_1\frac{m_7.q^\beta}{q^\beta+m_1}\right)\frac{m_7.q^\beta}{q^\beta+m_1}\overline{w}(\xi,q)&=\frac{P}{q}+\left(1+\lambda_2\frac{m_7.q^\beta}{q^\beta+m_1}\right)\frac{\partial^2\overline{w}(\xi,q)}{\partial\xi^2}\\-M\left(1+\lambda_1\frac{m_7.q^\beta}{q^\beta+m_1}\right)\overline{w}(\xi,q)-\frac{1}{K}\left(1+\lambda_2\frac{m_7.q^\beta}{q^\beta+m_1}\right)\overline{w}(\xi,q)&+Gr\overline{\Theta}(\xi,q)+Gm\overline{\Phi}(\xi,q),\end{aligned}\tag{55}$$

by solving the above equation using the Laplace and Fourier sine transforms to get the exact solutions. Using the same procedure for the solution of Eq. (55) and after applying the inverse Laplace and Fourier sine transform we get the following solution:

$$w(\xi,\tau)=\frac{2}{d}\sum_{N=1}^{\infty}(C(\tau))\sin\left(\frac{N\pi\xi}{h}\right)+\frac{2}{d}\sum_{N=1}^{\infty}\left[D(\tau)^*\left[Gr\Theta(\xi,\tau)+Gm\Phi(\xi,\tau)\right]\right]\sin\left(\frac{N\pi\xi}{h}\right).\tag{56}$$

The solution obtained in Eq. (56) is the limiting case in the absence of the couple stress effect.

5.2. Solution of maxwell fluid velocity

By putting the couple stress parameter $\eta=0$ and $\lambda_2=0$ our solutions of velocity profile reduced to Maxwell fluid. To find the solutions repeating the above mentioned process we get the solution of Maxwell fluid.

$$\begin{aligned}&\mathrm{Re}\left(1+\lambda_1\frac{m_7.q^\beta}{q^\beta+m_1}\right)\frac{m_7.q^\beta}{q^\beta+m_1}\overline{w}(\xi,q)=\frac{P}{q}+\frac{\partial^2\overline{w}(\xi,q)}{\partial\xi^2}\\&-M\left(1+\lambda_1\frac{m_7.q^\beta}{q^\beta+m_1}\right)\overline{w}(\xi,q)-\frac{1}{K}\overline{w}(\xi,q)+Gr\overline{\Theta}(\xi,q)+Gm\overline{\Phi}(\xi,q),\end{aligned}\tag{57}$$

using the same procedure as given in the solution of the momentum equation of the main problem. Applying both the Laplace and Fourier transforms to Eq. (57), the closed form solutions obtained:

$$w(\xi,\tau)=\frac{2}{d}\sum_{N=1}^{\infty}(E(\tau))\sin\left(\frac{N\pi\xi}{h}\right)+\frac{2}{d}\sum_{N=1}^{\infty}[F(\tau)^*[Gr\Theta(\xi,\tau)+Gm\Phi(\xi,\tau)]]\sin\left(\frac{N\pi\xi}{h}\right).\tag{58}$$

The Maxwell solution is given in Eq. (58).

5.3. Solution of Newtonian viscous fluid velocity

By taking the couple stress parameter $\eta=0$, $\lambda_1=0$ and $\lambda_2=0$ our solutions of velocity profile reduced to Newtonian viscous fluid. To find the solutions repeating the above-mentioned process we get the solution of Newtonian viscous fluid.

$$\begin{aligned}&\mathrm{Re}\frac{m_7.q^\beta}{q^\beta+m_1}\overline{w}(\xi,q)=\frac{P}{q}+\frac{\partial^2\overline{w}(\xi,q)}{\partial\xi^2}-M\overline{w}(\xi,q)\\&-\frac{1}{K}\overline{w}(\xi,q)+Gr\overline{\Theta}(\xi,q)+Gm\overline{\Phi}(\xi,q),\end{aligned}\tag{59}$$

Applying Fourier transform to Eq. (59), we get:

$$\begin{aligned}&\mathrm{Re}\frac{m_7.q^\beta}{q^\beta+m_1}\overline{w}_{Ns}(N,q)=\frac{P}{q}-\gamma_N^2\overline{w}_{Ns}(N,q)+\frac{\gamma_N}{q}-M\overline{w}_{Ns}(N,q)\\&-\frac{1}{K}\overline{w}_{Ns}(N,q)+Gr\overline{\Theta}_{Ns}(N,q)+Gm\overline{\Phi}_{Ns}(N,q),\end{aligned}\tag{60}$$

after some calculi Eq. (60), can be expressed as:

$$\overline{w}_{Ns}(N,q)=\frac{l_{15}(q^\beta+m_1)}{l_{12}.q(q^\beta+l_{14})}+\left[\frac{(q^\beta+m_1)}{l_{12}.q(q^\beta+l_{14})}\right]\times[Gr\overline{\Theta}_{Ns}(N,q)+Gm\overline{\Phi}_{Ns}(N,q)],\tag{61}$$

Equation (61) is obtained form the simplification of Eq. (60).

$$\overline{w}_{Ns}(N,q)=Q(q)+R(q)\times[Gr\overline{\Theta}_{Ns}(N,q)+Gm\overline{\Phi}_{Ns}(N,q)],\tag{62}$$

Applying the inverse Fourier and Laplace to Eq. (62), we get the following results:

$$w(\xi,\tau)=\frac{2}{d}\sum_{N=1}^{\infty}(Q(\tau))\sin\left(\frac{N\pi\xi}{h}\right)+\frac{2}{d}\sum_{N=1}^{\infty}[R(\tau)^*[Gr\Theta(\xi,\tau)+Gm\Phi(\xi,\tau)]]\sin\left(\frac{N\pi\xi}{h}\right).\tag{63}$$

Equation (63) shows the final solution of Newtonian viscous fluid.

5.4. Classical solution

In this subsection we highlight a special case of the present generalized model by taking $\beta\to1$ then the present obtained solutions reduced to the solution obtained by Akhtar, S., & Shah, N. A [44] which is the special case of the present solutions.

For the special case applying the property stated below:

$$\begin{aligned}\lim_{\beta\to1}{}^{AB}\mathbf{D}_\tau^\beta u(\xi,\tau)&=\lim_{\beta\to1}L^{-1}\left[L\left\{{}^{AB}\mathbf{D}_\tau^\beta u(\xi,\tau)\right\}\right]=L^{-1}\left\{\lim_{\beta\to1}\frac{q^\beta\overline{u}(\xi,q)-u(\xi,0)}{(1-\beta)q^\beta+\beta}\right\}\\&=L^{-1}\{q\overline{u}(\xi,q)-u(\xi,0)\}=L^{-1}[L\{u'(\xi,\tau)\}]=u'(\xi,\tau).\end{aligned}\tag{64}$$

The results obtained in Eq. (64) shows the classical results of the present fractional solution.

6. Liming case

6.1. Solution of CSF velocity

This section provides the limiting case of the present problem. Our solution can be reduced to already published work by putting $\lambda_1=0$ and $\lambda_2=0$ our solutions of velocity profile reduced to couple stress fluid CSF solutions obtained by Ali et al. [47] which verify our obtained solutions.

$$\mathrm{Re}\frac{m_7.q^{\beta}}{q^{\beta}+m_1}\overline{w}(\xi,q)=\frac{P}{q}+\frac{\partial^2\overline{w}(\xi,q)}{\partial\xi^2}-\eta\frac{\partial^4\overline{w}(\xi,q)}{\partial\xi^4}-M\overline{w}(\xi,q)$$
$$-\frac{1}{K}\overline{w}(\xi,q)+Gr\overline{\Theta}(\xi,q)+Gm\overline{\Phi}(\xi,q), \tag{65}$$

Applying the Fourier transform to Eq. (65), we get following transform result:

$$\mathrm{Re}\frac{m_7.q^{\beta}}{q^{\beta}+m_1}\overline{w}_{Ns}(N,q)=\frac{P}{q}-\gamma_N^2\overline{w}_{Ns}(N,q)+\frac{\gamma_N}{q}-\eta\gamma_N^4\overline{w}_{Ns}(N,q)+\frac{\gamma_N^3}{q}$$
$$-M\overline{w}_{Ns}(N,q)-\frac{1}{K}\overline{w}_{Ns}(N,q)+Gr\overline{\Theta}_{Ns}(N,q)+Gm\overline{\Phi}_{Ns}(N,q), \tag{66}$$

after some calculi Eq. (66), can be expressed as given in Eq. (67):

$$\overline{w}_{Ns}(N,q)=\frac{l_{11}(q^{\beta}+m_1)}{l_8.q(q^{\beta}+l_{10})}+\left[\frac{(q^{\beta}+m_1)}{l_8.q(q^{\beta}+l_{10})}\right]\times[Gr\overline{\Theta}_{Ns}(N,q)+Gm\overline{\Phi}_{Ns}(N,q)] \tag{67}$$

$$\overline{w}_{Ns}(N,q)=G(q)+H(q)\times[Gr\overline{\Theta}_{Ns}(N,q)+Gm\overline{\Phi}_{Ns}(N,q)], \tag{68}$$

To inverst the results obtained using the inverse of the Laplace and Fourier transform to Eq. (68), the results obtained is given below:

$$w(\xi,\tau)=\frac{2}{d}\sum_{N=1}^{\infty}(G(\tau))\sin\left(\frac{N\pi\xi}{h}\right)+\frac{2}{d}\sum_{N=1}^{\infty}[H(\tau)^*[Gr\Theta(\xi,\tau)+Gm\Phi(\xi,\tau)]]\sin\left(\frac{N\pi\xi}{h}\right). \tag{69}$$

The solutions obtained in Eq. (69) is identical to the solutions obtained by Ali et al. [31] which validate our work.
Where

$$\gamma_N=\left(\frac{N\pi}{d}\right),m_0=\frac{b_1}{1-\beta},m_1=\frac{\beta}{1-\beta},m_2=\frac{\gamma_N}{m_0+\gamma_N^2},m_3=\frac{\gamma_N^2.m_1}{m_0+\gamma_N^2},m_4=\frac{b_2}{1-\beta},m_5=\frac{\gamma_N}{m_4+\gamma_N^2},m_6=\frac{\gamma_N^2.m_1}{m_4+\gamma_N^2},m_7=\frac{1}{1-\beta},$$
$$m_8=1+\lambda_1m_7,m_9=\mathrm{Re}.m_8,m_{10}=\frac{m_1}{1+\lambda_1m_7},m_{11}=1+\lambda_2m_7,m_{12}=\frac{m_1}{1+\lambda_2m_7},m_{13}=\gamma_N^2+\frac{1}{K},m_{14}=\mathrm{Re}.m_7+\eta\gamma_N^4+M,$$
$$m_{15}=\frac{\eta.\gamma_N^4m_1+Mm_1}{m_{14}},m_{16}=P+\gamma_N.m_{11}+\eta.\gamma_N^3.m_8,m_{17}=\frac{P\cdot m_1+\gamma_N\cdot m_{11}m_{12}+\eta\cdot\gamma_N^3\cdot m_8\cdot m_{10}}{m_{16}},$$
$$m_{18}=m_8\cdot m_{14},m_{19}=m_{11}\cdot m_{13},m_{20}=m_{17}+m_1,m_{21}=m_1m_{17},m_{22}=m_{18}+m_{19},m_{23}=m_{15}m_{18}+m_{10}m_{18}+m_1m_{19}+m_{12}m_{19},$$
$$m_{24}=m_1m_{12}m_{19}\ .$$

$$b_1=\mathrm{Re}.m_7+M,b_2=\frac{Mm_1}{b_1},b_3=P+\gamma_N.m_{11},b_4=\frac{P\cdot m_1+\gamma_N\cdot m_{11}m_{12}}{b_3},b_5=m_8\cdot b_1,b_6=m_{11}\cdot m_{13},b_7=b_4+m_1,b_8=m_1b_4,b_9$$
$$=b_5+b_6,b_{10}=b_2b_5+m_{10}b_5+m_1b_6+m_{12}b_6,b_{11}=m_1m_{12}b_6\ .$$

$$l_1=P+\gamma_N+\eta.\gamma_N^3.m_8,l_2=\frac{P\cdot m_1+\gamma_N\cdot m_1+\eta\cdot\gamma_N^3\cdot m_8\cdot m_{10}}{l_1},l_3=l_2+m_1,l_4=m_1l_2,l_5=m_{18}+m_{13},l_6$$
$$=m_{15}m_{18}+m_{10}m_{18}+m_1m_{13}+m_1m_{13},l_7=m_1^2m_1,$$

$$l_8=\mathrm{Re}m_7+\gamma_N^2+\eta.\gamma_N^4+M+\frac{1}{K},l_9=m_1.\left(\gamma_N^2+\eta.\gamma_N^4+M+\frac{1}{K}\right),l_{10}=\frac{l_9}{l_8},l_{11}=P+\gamma_N+\eta\gamma_N^3,$$

$$l_{12}=\mathrm{Re}m_7+\gamma_N^2+M+\frac{1}{K},l_{13}=m_1.\left(\gamma_N^2+M+\frac{1}{K}\right),l_{14}=\frac{l_{13}}{l_{12}},l_{15}=P+\gamma_N\ .$$

7. Nusselt number, sherwood number and skin friction

In this section we provide the engineering quantities for the present problem. The engineering quantities are the Nusselt number given in subsection 6.1, Sherwood number given 6.2 and the corresponding skin friction is given in 6.3.

7.1. Evaluation of nusselt number

The expression for the engineering values of Nusselt number for Oldroyd-B couple stress fluid can be expressed as:

$$Nu=-\left.\frac{\partial\Theta}{\partial\xi}\right|_{\xi=0}. \tag{70}$$

7.2. Evaluation of sherwood number

The expression of the corresponding Sherwood number for engineering quantities for Oldroyd-B couple stress fluid can be written as:

$$Sh = -\left.\frac{\partial \Phi}{\partial \xi}\right|_{\xi=0}. \tag{71}$$

7.3. Skin friction

The Skin friction for the given fluid is given below:

$$Sf(\xi,\tau) = (1+\lambda_1)\left(\frac{\partial w}{\partial \xi} - \eta\frac{\partial^3 w}{\partial \xi^3}\right). \tag{72}$$

The skin friction for the left and right plate is calculated by using the following expressions:

$$Sf_{lp}(0,\tau) = (1+\lambda_1)\left(\frac{\partial w}{\partial \xi} - \eta\frac{\partial^3 w}{\partial \xi^3}\right)_{\xi=0}, \tag{73}$$

where $Sf_{lp}(.)$ represents the notation of skin friction at left plate.

$$Sf_{rp}(1,\tau) = (1+\lambda_1)\left(\frac{\partial w}{\partial \xi} - \eta\frac{\partial^3 w}{\partial \xi^3}\right)_{\xi=1}. \tag{74}$$

Where $Sf_{rp}(.)$ represents the notation of skin friction at right plate.

The engineering quantities are mentioned in Eqs.70–74, which can be used in many engineering problems.

8. Results and discussion

This section provides the graphical analysis of unsteady MHD Oldroyd-B fluid with couple stress effect along with energy and concentration effect. The Oldroyd-B fluid is allowed to pass through channel with porosity effect. The aims of this portion to visualize the flow behavior of the parameters involved during the flow. The simple classical models were unable to explained the complex nature of non-Newtonian fluid model in order to highlight these complex models in the present study newly developed AB time fractional order derivative is applied on the classical model and we get the generalized model which highlight the sensitive memory effect on the fluid dynamics. The exact results obtained from the present study by applying the integral transforms (Laplace and Fourier). For clear understanding all the flow parameters are highlighted through graphs and discussed in detail. Graphically, the impact of these flow parameters have evaluated on the fluid flow. The involved flow parameters in the present analysis are Grashof and modified Grashof numbers are Gr and Gm respectively, M, Pr, Sc, Re, K, λ_1, λ_2, P, η and β, magnetic parameter, Prandtl number, Schmidt number, Reynolds number, porous media, relaxation, retardation parameter, pressure, couple stress parameter, and fractional parameter respectively. All these parameters are involved in the skin, friction, Nusselt and Sherwood number for engineering purposes and presented in tabular forms. Furthermore, the present solutions of the Oldroyd-B fluid model with couple stresses have been reduced to simple Oldroyd-B without couple stresses, Maxwell fluid, couple stress fluid and Newtonian viscous fluid as a special case. All the above-mentioned solutions have been compared in order to observe the flow analysis of the present model deeply. Finally, all the above solutions are plotted for classical and AB fractional derivatives and compared their results.

The physical sketch can be visualized in Fig. 1 (a) and the solution methodology of the current research is depicted in Fig. 1(b). The fractional parameter β on MHD Oldroyd-B fluid with couple stresses is portrayed in Fig. 2. The present figure clearly elucidated, and we found that greater values of fractional parameter β shows multiple solutions of Oldroyd-B fluid with couple stresses which is referred as memory effect of fractional parameter on the fluid flow. In the case if an experimentalist wants to compare their obtained results with our theoretical results for the fluid motion, he can chose any arbitrary values of β for the required results. Furthermore, for $\beta = 1$ shows the classical solution of the present model. The impact time τ on the velocity of the fluid is portrayed in Fig. 3. The Oldroyd-B couple stress fluid is a type of non-Newtonian fluid that exhibits additional viscoelastic properties due to the presence of microstructures within the fluid. In a channel, the flow behavior of the Oldroyd-B couple stress fluid can be affected by several factors, including the velocity profile, the geometry of the channel, the presence of walls or obstacles. One important factor that can significantly impact the flow behavior of the Oldroyd-B couple stress fluid in a channel is time. Specifically, the way the fluid responds to changes in the flow conditions can vary depending on how long the fluid has been flowing. During the present analysis it has been noticed that higher the time the velocity of the fluid within the channel get high.

Fig. 4 shows the influence of external pressure P on the fluid motion in channel. From the figure it can be notice clearly that by increasing the external pressure lead to an increase in the Oldroyd-B fluid motion in channel because the external pressure is responsible to accelerate the fluid motion. Physically, it is correct when a pressure gradient is applied to an Oldroyd-B couple stress fluid flowing in a channel, the velocity of the fluid is affected by both the viscosity and the elastic properties of the fluid. The increase in pressure gradient generates a shear stress on the fluid. This applied pressure on the velocity of the Oldroyd-B couple stress fluid in a

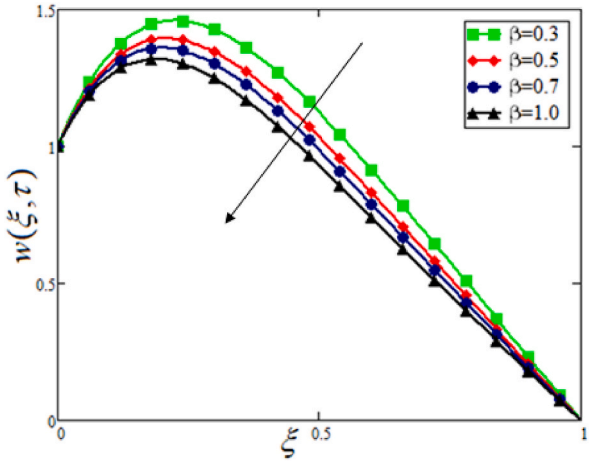

Fig. 2. The velocity of fluid versus different values of β.

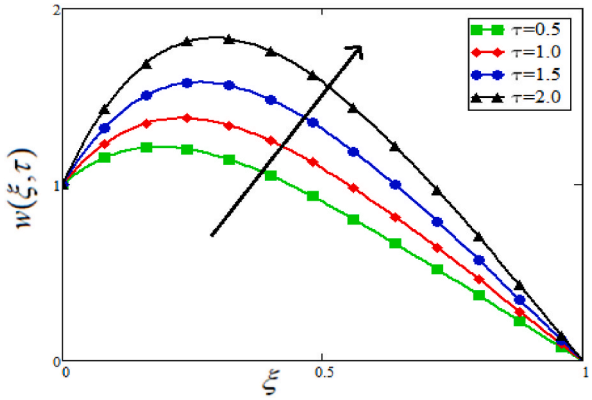

Fig. 3. The velocity of fluid versus different values of τ.

channel is thus affected by both the viscous forces and the elastic forces within the fluid. In our case as the pressure gradient increases, the viscous forces become weaker, and the elastic forces become stronger as a result it tend to push the fluid forward. Therefore higher the pressure will accelerate the velocity of the fluid in channel. The influence of M on the velocity of MHD Oldroyd-B couple stress fluid is portrayed in Fig. 5. This plot can easily described that when we choose higher numerical values of M as a result it produces some resistivity opposite in the fluid motion. These resistive forces become stronger for greater values of M which is called as the Lorentz forces. Therefore, for higher values of M the Lorentz forces become stronger which retard the fluid motion. In conclusion, when higher

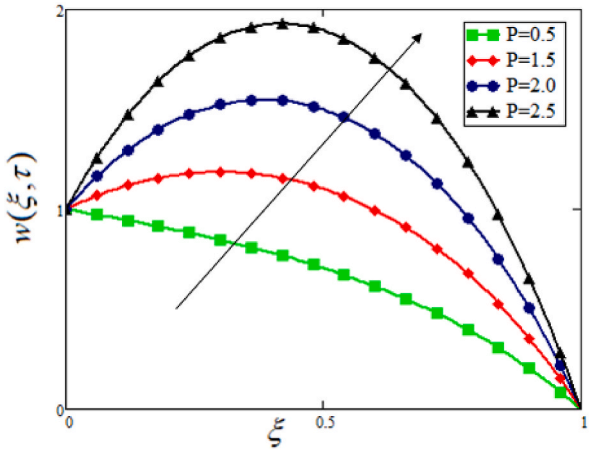

Fig. 4. The velocity of fluid versus different values of P.

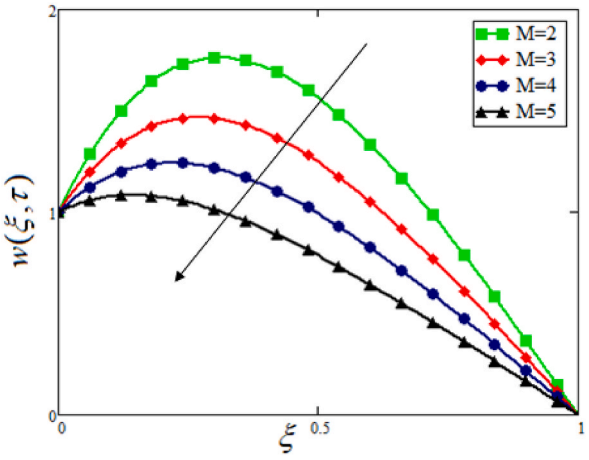

Fig. 5. The velocity of fluid versus different values of *M*.

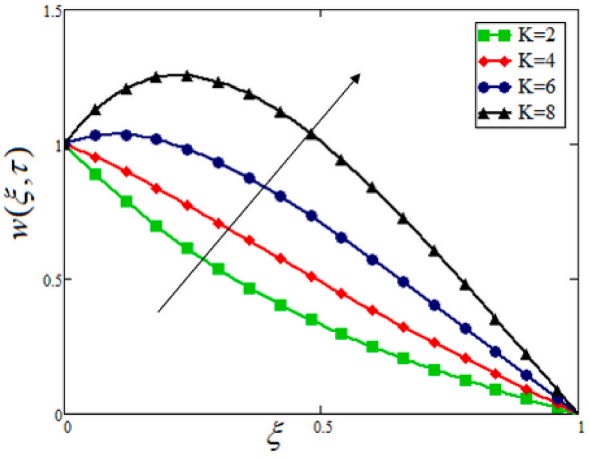

Fig. 6. The velocity of fluid versus different values of *K*.

values of *M* is taken Lorentz forces become stronger and as a result fluid motion retard and hence velocity of the fluid decreases.

Fig. 6 visualizes the presence of porous media *K* when the fluid is in motion in channel. This figure depicted that when the fluid passing through the region where porosity is higher shows low opposing forces in the fluid direction. Therefore, for the increasing the porosity *K* there is low resistance in the fluid flow and hence velocity of the fluid increases. This shows that as we increases the pores of the medium as a results the fluid passing through the porous media will have low resistive forces between the fluid and surface

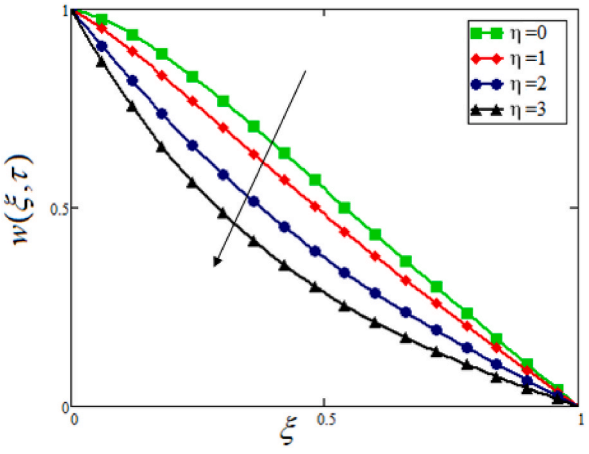

Fig. 7. The velocity of fluid versus different values of *η*.

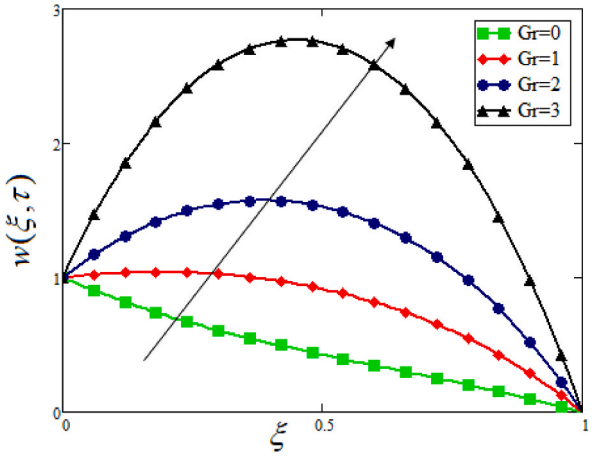

Fig. 8. The velocity of fluid versus different values of *Gr*.

consequently, the fluid will get higher magnitude. Physically it is correct because when a fluid flows through a porous medium, it experiences resistance due to the presence of small, interconnected pores in the medium. This resistance leads to a reduction in the fluid velocity compared to the same fluid flowing in a non-porous medium. Therefore, increasing the pores of the medium will ultimately reduced the resistance in the flow direction and hence the fluid velocity get higher in channel. The presence of couple stress parameter η on the fluid motion is portrayed in Fig. 7. Here an increase in the η means that where going to high the viscosity of the fluid as a result more viscosity the fluid have will low velocity. Therefore, during the graphical analysis one can noticed that increasing the couple stresses in the fluid the velocity of the Oldroyd-B fluid decreases because the couple stresses effects the fluid motion due to its couple shear stresses which are responsible to retard the fluid motion flowing in the channel. The physical reason behind it is that the Oldroyd-B couple stress fluid is a type of non-Newtonian fluid that exhibits unique properties due to the presence of a couple stress parameter. This parameter measures the effect of micro-scale rotations or internal angular momentum of fluid particles on the overall behavior of the fluid. When the couple stress parameter is increased, the velocity profile of the Oldroyd-B fluid in a channel changes significantly. Specifically, the presence of the couple stress parameter can lead to the development of secondary flows, such as vortices and eddies, within the channel. These secondary flows can significantly alter the overall velocity distribution of the fluid and result in complex fluid behavior. Therefore, increasing the CSF parameter develop complexity in the fluid due to which velocity of the fluid retards in channel. Furthermore, for $\eta = 0$ shows a special case of having no couple shear stresses on the fluid flow. Figs. 8 and 9 portrayed the flow parameters thermal and mass Grashof number *Gr* and *Gm* respectively. The graphical representations of these buoyancy parameters visualizes its impact on the dynamics of fluid and it can be observed that higher the these values will get high the amplitude of velocity because these buoyancy forces are responsible to accelerate the fluid motion in the boundary layer region. From these figures one can noticed that buoyancy forces are dominant on viscous forces as a result the fluid velocity increase for higher values of these buoyancy forces. The thermal Grashof number and mass Grashof number are two important dimensionless parameters that are used to describe the behavior of fluids in various flow systems, including channels. In the case of Oldroyd-B couple stress fluid in a channel, these parameters can have a significant impact on the velocity distribution of the fluid. The increase in both the parameters causes an acceleration in the velocityof the fluid. Physically, it is correct, because *Gr* is increased, the buoyancy forces become

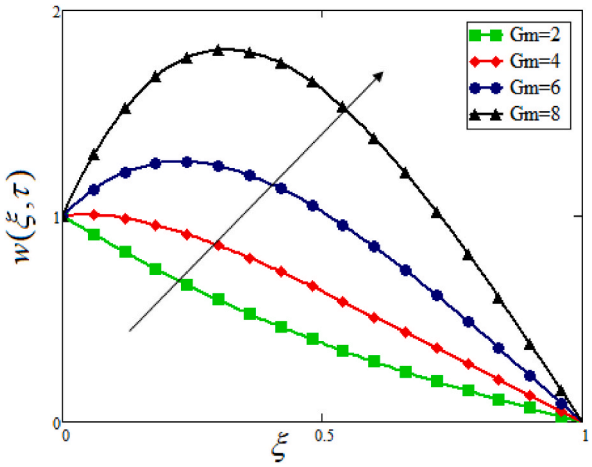

Fig. 9. The velocity of fluid versus different values of *Gm*.

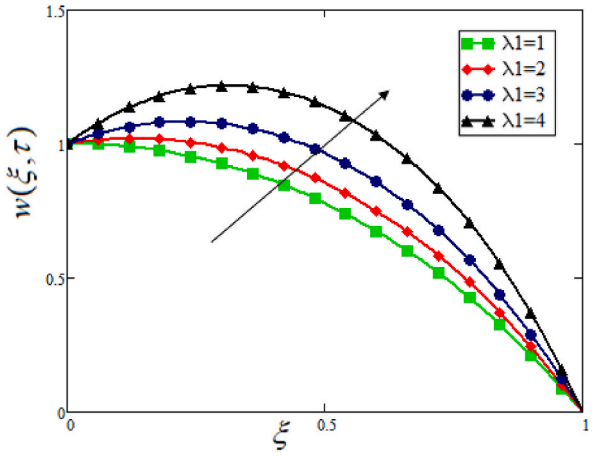

Fig. 10. The velocity of fluid versus different values of λ_1.

more dominant, leading to the formation of thermal plumes and the development of convective flows. In the case of Oldroyd-B fluids, these convective flows can interact with the couple stress effects and result in complex velocity distributions. The presence of the couple stress parameter can also affect the onset of convection and the strength of the convective flow. Therefore, the over all impact of the thermal and mass Grashof numbers on the velocity distribution of Oldroyd-B couple stress fluids in channels have an increasing effect in the velocity.

Fig. 10 Shows the trends of time relaxation parameter λ_1 and its impact the motion of fluid in channel. This graphical sketch of the flow for λ_1 depicts that when we choose the high numerical values of λ_1 as a result there is an increase cam be noticed in the fluid velocity in channel. This increment in the velocity physically corrects because normally, relaxation time parameter in the Oldroyd-B model that characterizes the timescale over which the elastic stresses in the fluid relax. In particular, it measures the time required for the fluid to return to its undeformed state after a deformation has been applied. In a channel flow, the velocity profile of an Oldroyd-B fluid is influenced by the relaxation time parameter in a few different ways. In some case when there is a smaller relaxation times result in a more elastic fluid, which tends to resist deformation more strongly. This can lead to a reduction in the fluid velocity, particularly near the walls of the channel where the flow is most strongly affected by the fluid's elastic properties. Similarly, when larger relaxation times, on the other hand, result in a more viscous fluid, which tends to flow more easily. This can lead to an increase in the fluid velocity, particularly in the center of the channel where the flow is less influenced by the fluid's elastic properties. This is the reason that increasing λ_1 lead to an increase in the fluid velocity.

The trends in flow pattern are highlighted in the time retardation parameter λ_2 and presented in Fig. 11 on the flow profile of the fluid. This figure visualized that higher magnitude of λ_2 a decreasing behavior is noticed in the flow pattern. Physically, it is correct because in a channel flow of an Oldroyd-B fluid, the retardation time parameter affects the velocity profile of the fluid. When the values of λ_2 is small, the fluid recovers its elastic properties quickly, and the velocity profile is more uniform. However, as λ_2 increases, the fluid takes longer to recover its elastic properties, and the velocity profile becomes more complex, with regions of high and low velocities. Specifically, for a channel flow of an Oldroyd-B fluid, when the retardation time is small, the fluid behaves more like a Newtonian fluid, where the velocity profile is linear and the shear rate is proportional to the velocity gradient. As the retardation time

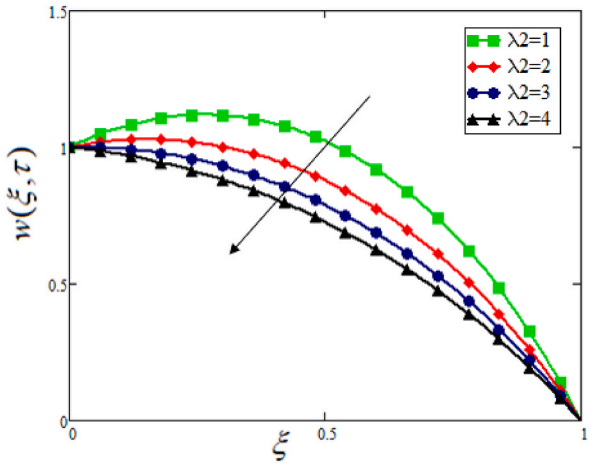

Fig. 11. The velocity of fluid versus different values of λ_2.

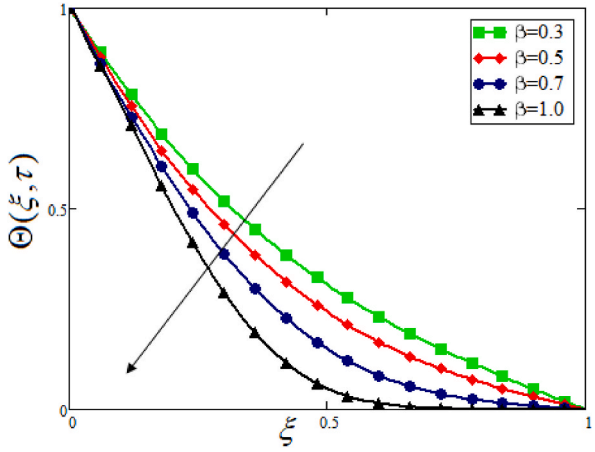

Fig. 12. The temperature of fluid versus different values of β.

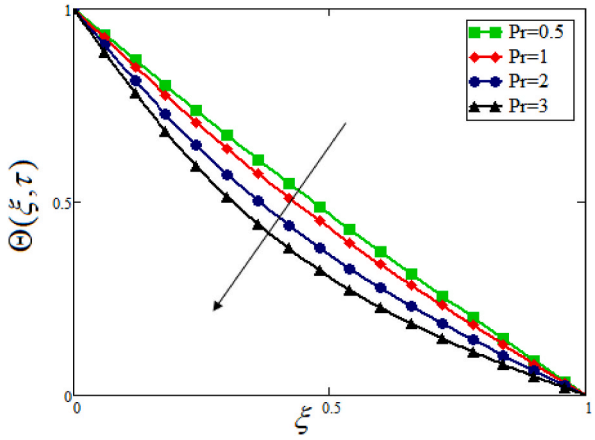

Fig. 13. The temperature of fluid versus different values of Pr.

increases, the fluid becomes more viscoelastic, with a curved velocity profile and a non-linear relationship between the shear rate and the velocity gradient. This is the reason when λ_2 is high the velocity decelerated in channel. Furthermore, it can be noticed that the time relaxation parameter λ_1 and time retardation parameter λ_2 have opposite behavior on the fluid velocity they have an inverse relation with velocity and it can be observed from the main momentum equation from the mathematical modeling and solution section.

Fig. 12 depicts the presence of AB fractional parameter β on temperature distribution of the fluid. The diagram clearly visualized

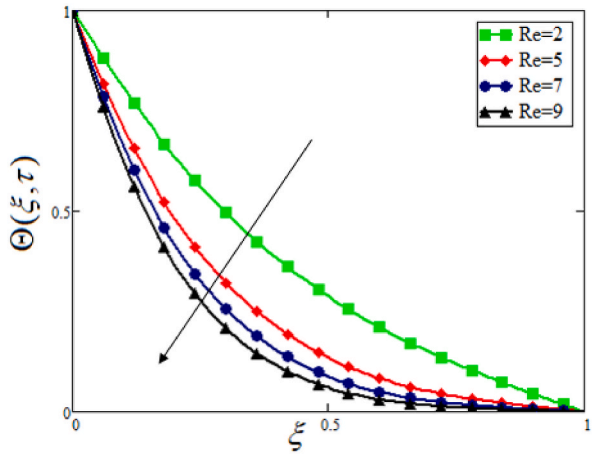

Fig. 14. The temperature of fluid versus different values of Re.

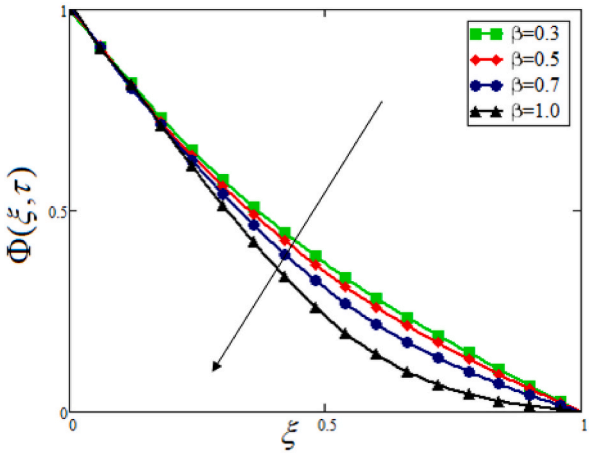

Fig. 15. The concentration of fluid versus different values of β.

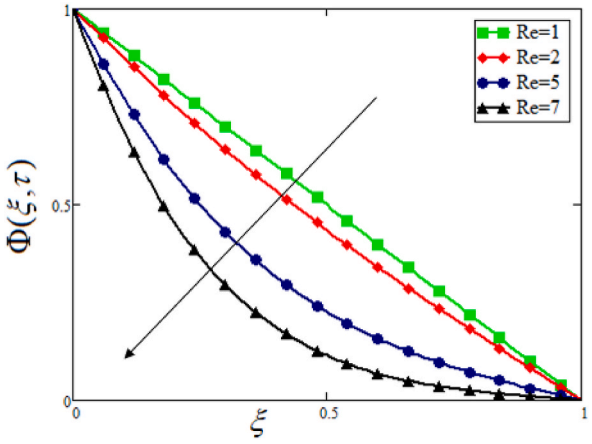

Fig. 16. The concentration of fluid versus different values of Re.

that choosing the high values of β make their temperature lower, this concluded that for different β we have variation in temperature. In some real-life system temperature cannot be examined correctly by applying simple classical derivative approach therefore, for better results of temperature fractional derivative is used to analyze temperature in different operating systems.

The trends in temperature of the flow for various values of Pr presented in Fig. 13. The variation occur in temperature profile for choosing high values of Pr. This variation is noticed that keeping high Pr values the temperature get lower. This decrease occur in

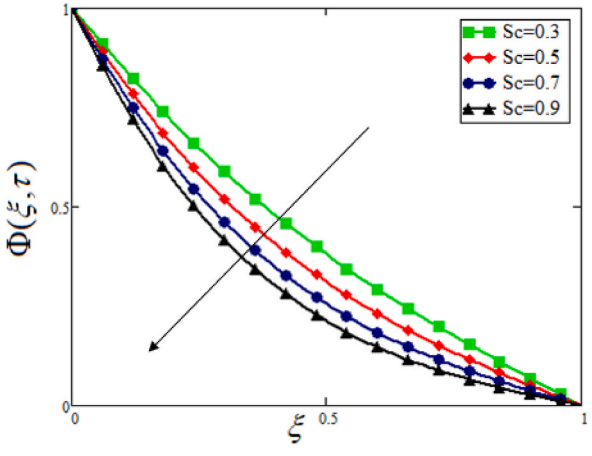

Fig. 17. The concentration of fluid versus different values of *Sc*.

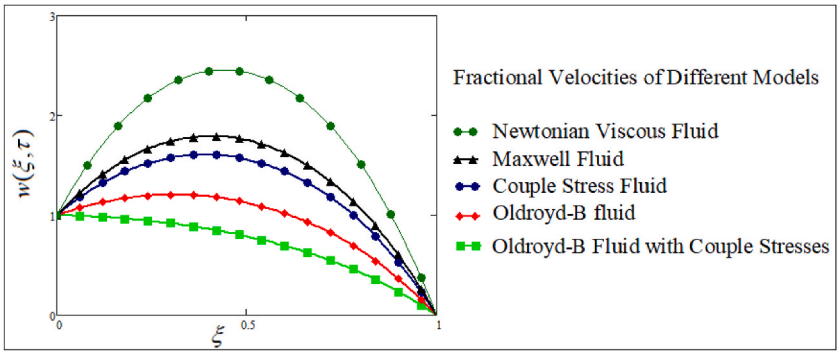

Fig. 18. The comparative graphical analysis of the solutions of fractional Oldroyd-B fluid velocity with Maxwell fluid, couple stress fluid and Newtonian viscous fluid velocity.

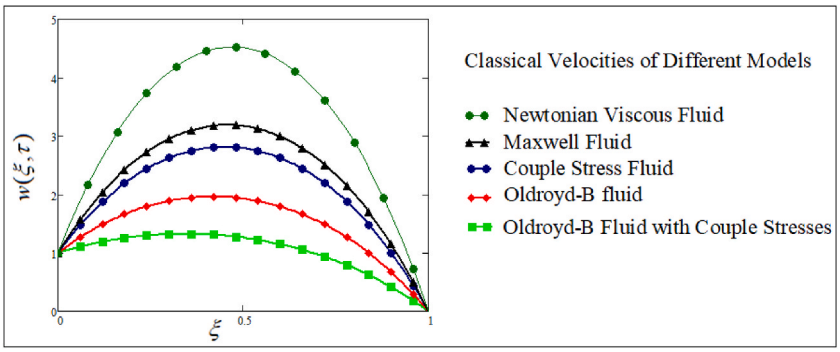

Fig. 19. The comparative graphical analysis of the solutions of classical Oldroyd-B fluid velocity with Maxwell fluid, couple stress fluid and Newtonian viscous fluid velocity.

temperature it is because Pr represents here the ratios among momentum and thermal diffusivity. This means that high the Pr values will off course increase the thermal conductivity of the fluid as result fluid temperature decreases. The impact of Reynolds number Re on temperature of the flow visualizes in Fig. 14. This diagram depicted and one can observe that choosing maximum values of *Re* the temperature of the fluid get lowered.

The AB fractional parameter β and its impact on concentration profile is presented in Fig. 15. This graphically, described that the positive change produces in β the concentration get lowered it is because varying β we have variation in concentration. In some real-life system concentration cannot be examined correctly by applying simple classical derivative approach therefore, for better results of concentration fractional derivative is used to analyze concentration of the fluid. Fig. 16 portrayed the presence of Re on the concentration of the Oldroyd-B fluid. From this sketch it is clear that when considering the high values of Re result a decrement in the

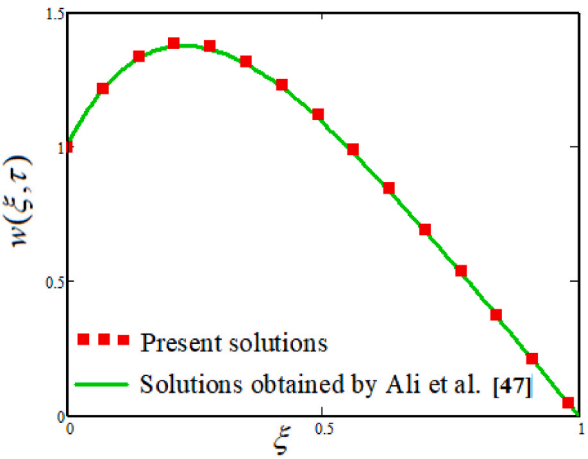

Fig. 20. The comparative analysis of the present solutions with the solutions obtained by Ali et al. [47].

Table 1
The skin friction variation against different parameters Oldroyd-B couple stress fluid at left plate.

β	λ_1	λ_2	τ	Gr	Gm	Pr	Sc	M	K	η	P	Re	$Sf_{left\ plate}$
0.5	0.8	2	1.2	12	8	15	2.5	2.1	1.5	2.2	3	2.5	4.0631
0.7	0.8	2	1.2	12	8	15	2.5	2.1	1.5	2.2	3	2.5	3.2375
0.5	**1.2**	2	1.2	12	8	15	2.5	2.1	1.5	2.2	3	2.5	5.2402
0.5	0.8	**2.5**	1.2	12	8	15	2.5	2.1	1.5	2.2	3	2.5	3.821
0.5	0.8	2	**1.5**	12	8	15	2.5	2.1	1.5	2.2	3	2.5	6.0592
0.5	0.8	2	1.2	**15**	8	15	2.5	2.1	1.5	2.2	3	2.5	5.8743
0.5	0.8	2	1.2	12	**10**	15	2.5	2.1	1.5	2.2	3	2.5	5.2751
0.5	0.8	2	1.2	12	8	**20**	2.5	2.1	1.5	2.2	3	2.5	3.9281
0.5	0.8	2	1.2	12	8	15	**3**	2.1	1.5	2.2	3	2.5	3.0321
0.5	0.8	2	1.2	12	8	15	2.5	**2.5**	1.5	2.2	3	2.5	3.0582
0.5	0.8	2	1.2	12	8	15	2.5	2.1	**2**	2.2	3	2.5	5.8573
0.5	0.8	2	1.2	12	8	15	2.5	2.1	1.5	**2.5**	3	2.5	3.0825
0.5	0.8	2	1.2	12	8	15	2.5	2.1	1.5	2.2	**4**	3.5	5.7352
0.5	0.8	2	1.2	12	8	15	2.5	2.1	1.5	2.2	3	**4.5**	3.7352

Table 2
The skin friction variation against different parameters Oldroyd-B couple stress fluid at right plate.

β	λ_1	λ_2	τ	Gr	Gm	Pr	Sc	M	K	η	P	Re	$Sf_{right\ plate}$
0.5	0.8	2	1.2	12	8	15	2.5	2.1	1.5	2.2	3	2.5	2.0631
0.7	0.8	2	1.2	12	8	15	2.5	2.1	1.5	2.2	3	2.5	1.2375
0.5	**1.2**	2	1.2	12	8	15	2.5	2.1	1.5	2.2	3	2.5	3.2402
0.5	0.8	**2.5**	1.2	12	8	15	2.5	2.1	1.5	2.2	3	2.5	2.921
0.5	0.8	2	**1.5**	12	8	15	2.5	2.1	1.5	2.2	3	2.5	3.592
0.5	0.8	2	1.2	**15**	8	15	2.5	2.1	1.5	2.2	3	2.5	3.9743
0.5	0.8	2	1.2	12	**10**	15	2.5	2.1	1.5	2.2	3	2.5	3.2751
0.5	0.8	2	1.2	12	8	**20**	2.5	2.1	1.5	2.2	3	2.5	1.9281
0.5	0.8	2	1.2	12	8	15	**3**	2.1	1.5	2.2	3	2.5	1.0321
0.5	0.8	2	1.2	12	8	15	2.5	**2.5**	1.5	2.2	3	2.5	1.0582
0.5	0.8	2	1.2	12	8	15	2.5	2.1	**2**	2.2	3	2.5	3.8573
0.5	0.8	2	1.2	12	8	15	2.5	2.1	1.5	**2.5**	3	2.5	1.0825
0.5	0.8	2	1.2	12	8	15	2.5	2.1	1.5	2.2	**4**	3.5	3.7352
0.5	0.8	2	1.2	12	8	15	2.5	2.1	1.5	2.2	3	**4.5**	1.7352

Table 3
The impact of Nusselt number against different parameters.

β	τ	Pr	Re	$Nu_{Left\ \ Plate}$
0.5	1	14	2.5	1.511
0.7	1	14	2.5	1.061
0.5	**1.5**	14	2.5	1.424
0.5	1	**16**	2.5	1.848
0.5	1	14	**3**	1.654

Table 4
The impact of Sherwood number against different parameters.

β	τ	Sc	Re	$Sh_{Left\ \ Plate}$
0.5	1.2	0.8	2.2	0.9
0.7	1.2	0.8	2.2	0.493
0.5	**1.5**	0.8	2.2	0.894
0.5	1.2	**1.2**	2.2	0.938
0.5	1.2	0.8	**3**	0.925

concentration. Fig. 17 visualizes the role of Schmidt number Sc on concentration distribution. This graph shows the presence of Sc on the fluid concentration and one can observed that Sc is responsible to reduce the concertation profile.

Fig. 18 shows the comparison of the velocity of MHD Oldroyd-B couple stress fluid with the simple Oldroyd-B fluid without couple stresses, couple stress fluid, Maxwell fluid and Newtonian viscous fluid. From the comparison we can see that magnitude of Newtonian viscous fluid velocity is higher than all the other fluid velocities and Oldroyd-B couple stress fluid velocity have low velocity compared to all other fluid velocity. The aim of this comparison is that the present solution can be viewed deeply by comparing with the Maxwell fluid, couple stress fluid and simple Newtonian viscous fluid. Additionally, Figs. 18 and 19 shows the same comparison for classical and fractional approach respectively. The comparison of the present obtained solutions with the already published work by Ali et al. [47] is highlighted in Fig. 20. According to the figure the present solutions shows a strong agreement with the published work as a limiting case which validate our solutions.

Tables 1 and 2 shows the skin friction of left and right plate for the different values of all parameters which effect the fluid flow. From the tables we can see the bold values in each specific row, which shows the changes occur in the skin friction for that specific bold value. Similarly, the influence of different parameters on the Nusselt number are evaluated and presented in Table 3. Finally, Table 4 shows the effect of parameters on the Sherwood number which are calculated and presented in tabular form.

9. Conclusion

The purpose of this study is to expand upon existing research by investigating a larger class of fluid, specifically the Oldroyd-B couple stress fluid. The study aims to develop a generalized form of this fluid with the inclusion of an extra couple stress effect in a channel. The study also considers the effect of heat and mass transfer on the fluid passing through the channel, as well as the external pressure effect on fluid flow. The classical model is adapted using the AB fractional operator, resulting in a fractional model system of equations. The study examines the impact of MHD and porosity on the system. Closed-form results for flow, temperature, and concentration are obtained by utilizing integral transforms such as Laplace and Fourier transforms. Additionally, limiting cases are calculated and compared with the original solution to critically analyze the flow behavior of the presented study. The obtained limiting solutions are also compared using classical and AB fractional approaches. Moreover, the present results have been reduced to already published work which verify our obtained solutions. The impact of all flow parameters on flow, heat, and concentration are illustrated and presented in figures. Numerical results for engineering purposes, such as skin friction, Nusselt number, and Sherwood number, are obtained and presented in tables. The impact of all the parameters involved in these engineering quantities is calculated and listed in the tables. Some important findings from this study are extracted and presented.

- The flow, heat and concentration profiles get lower for the increasing values of β and when the classical case $\beta = 1$ is considered the velocity, temperature and concertation profile is lowest.
- The exact solutions have been obtained for the new class of fluid namely Oldroyd-B fluid with couple stresses.
- The increasing values of time relaxation λ_1 accelerate the fluid velocity while the time retardation parameter λ_2 retards the fluid flow. The influence of λ_1 and λ_2 are opposite because they have inverse variation with the velocity of the fluid.
- The velocity of the magnetohydrodynamics Oldroyd-B fluid with couple stresses in porous media decreases for the greater values of fractional parameter β, M, η and λ_2.
- The velocity of fluid get high with the increment of numeric values of P, K, Gr, Gm and λ_1.
- The temperature gets lower for high values of Pr, Re and β.
- The concentration gets lower for higher values of Sc, Re and β.
- A breif comparison between different fluid models have been done for classical and fractional derivatives

10. Future direction

The present analysis holds promise for future research in several ways. The main novelty of this study can be further explored and expanded upon by considering the following possibilities.

- The current model can be extended by incorporating boundary conditions such as slip and no-slip conditions, mass flux, variable temperature and concentration at the boundary, among others.
- The present model can extend by taking different initial and boundary conditions.
- The present model can extend by considering the nanofluid and hybrid nanofluid model with different base fluid.
- The present model can be highlighted in terms of a very new idea of tri-hybrid nanofluid and can be applied to different base fluids, such as water, engine oil, transformer oil, blood, kerosene oil, honey, etc., by considering the mixture of three different types of nanoparticles.
- This model can extend by applying various fractional operator and highlight the impact of different fractional derivatives on the fluid flow.
- While this research focuses on flow of Oldroyd-B fluid with couple stresses in a channel, the future studies can explore different types of non-Newtonian fluid flow models, such as Casson fluid, Maxwell fluid, and Jeffery fluid, etc.
- Future research can also involve the use of different nanoparticles for different scientific purposes.
- To expand the scope of this study, one can extend the present model by using stretching sheet, inclined plate, stretching cylinder, rotating frame and cavity problems, etc.

Funding statement

This research did not receive any specific grant or funding.

Author contribution statement

1) conceived and designed the experiments;
2) performed the experiments;
3) analyzed and interpreted the data;

4) contributed reagents, materials, analysis tools or data;
5) wrote the paper.

Data availability statement

Data included in article/supplementary material/referenced in article.

Declaration of competing interest

The authors declare that they have no known competing financial interests or personal relationships that could have appeared to influence the work reported in this paper.

Acknowledgment

The authors acknowledge the financial support provided by the Center of Excellence in Theoretical and Computational Science (TaCS-CoE), KMUTT. Moreover, this research project is supported by Thailand Science Research and Innovation (TSRI) Basic Research Fund: Fiscal year 2022 (FF65). The first author Muhammad Arif appreciate the support provided by Petchra Pra Jom Klao Ph.D. Research Scholarship (Grant No. 14/2562 and Grant No. 25/2563).

The authors acknowledge the financial support provided by the Center of Excellence in Theoretical and Computational Science (TaCS-CoE), KMUTT. This research was funded by National Science, Research and Innovation Fund (NSRF), King Mongkut's University of Technology North Bangkok with Contract no. KMUTNB–FF–66-36.

References

[1] J.G. Oldroyd, On the formulation of rheological equations of state, Proc. R. Soc. London, A 200 (1063) (1950) 523–541, http://dx.doi.org/10.1098/rspa.1950.0035.
[2] R. Razzaq, U. Farooq, J. Cui, T. Muhammad, Non-similar solution for magnetized flow of Maxwell nanofluid over an exponentially stretching surface, Math. Probl Eng. (2021) 2021, http://dx.doi.org/10.1155/2021/5539542.
[3] S. Prema, B.M. Shankar, K.N. Seetharamu, Convection heat transfer in a porous medium saturated with an Oldroyd B fluid-A Review, February) p. 012029), J. Phys. Conf. 1473 (No. 1) (2020), http://dx.doi.org/10.1088/1742-6596/1473/1/012029. IOP Publishing.
[4] S.E.E. Hamza, MHD flow of an Oldroyd–B fluid through porous medium in a circular channel under the effect of time dependent pressure gradient, Am. J. Fluid Dynam. 7 (1) (2017) 1–11, http://dx.doi.org/10.5923/j.ajfd.20170701.01.
[5] C. Fetecau, S.C. Prasad, K.R. Rajagopal, A note on the flow induced by a constantly accelerating plate in an Oldroyd-B fluid, Appl. Math. Model. 31 (4) (2007) 647–654, http://dx.doi.org/10.1016/j.apm.2005.11.032.
[6] C. Fetecau, T. Hayat, M. Khan, Unsteady flow of an Oldroyd-B fluid induced by the impulsive motion of a plate between two side walls perpendicular to the plate, Acta Mech. 198 (1) (2008) 21–33, http://dx.doi.org/10.1007/s00707-007-0522-0.
[7] A. Elhanafy, A. Guaily, A. Elsaid, Numerical simulation of Oldroyd-B fluid with application to hemodynamics, Adv. Mech. Eng. 11 (5) (2019), 1687814019852844, http://dx.doi.org/10.1177/1687814019852844.
[8] M. Tahir, M.N. Naeem, M. Javaid, M. Younas, M. Imran, N. Sadiq, R. Safdar, Unsteady flow of fractional Oldroyd-B fluids through rotating annulus, Open Phys. 16 (1) (2018) 193–200, http://dx.doi.org/10.1515/phys-2018-0028.
[9] K. Mahmud, R. Mehmood, S. Rana, A. Al-Zubaidi, Flow of magnetic shear thinning nano fluid under zero mass flux and hall current, J. Mol. Liq. 352 (2022), 118732, http://dx.doi.org/10.1016/j.molliq.2022.118732.
[10] R. Mehmood, S. Rana, O. Anwar Bég, A. Kadir, Numerical study of chemical reaction effects in magnetohydrodynamic Oldroyd-B: oblique stagnation flow with a non-Fourier heat flux model, J. Braz. Soc. Mech. Sci. Eng. 40 (2018) 1–14, http://dx.doi.org/10.1007/s40430-018-1446-4.
[11] V.K. Stokes, Couple stresses in fluids, in: Theories of Fluids with Microstructure, Springer, Berlin, Heidelberg, 1984, pp. 34–80.
[12] V.K. Stokes, Theories of Fluids with Microstructure: an Introduction, Springer Science & Business Media, 2012.
[13] M. Arif, F. Ali, I. Khan, K.S. Nisar, A time fractional model with non-singular kernel the generalized Couette flow of couple stress nanofluid, IEEE Access 8 (2020) 77378–77395, http://dx.doi.org/10.1109/ACCESS.2020.2982028.
[14] G.J. Reddy, M. Kumar, H.P. Rani, Study of entropy generation in transient hydromagnetic flow of couple stress fluid due to heat and mass transfer from a radiative vertical cylinder, Pramana 93 (2019) 1–14, http://dx.doi.org/10.1007/s12043-019-1861-9.
[15] M. Kumar, G.J. Reddy, N.N. Kumar, O.A. Bég, Application of differential transform method to unsteady free convective heat transfer of a couple stress fluid over a stretching sheet, Heat Tran. Asian Res. 48 (2) (2019) 582–600, http://dx.doi.org/10.1002/htj.21396.
[16] H. Basha, G.J. Reddy, N.V. Narayanan, O.A. Bég, Supercritical heat transfer characteristics of couple stress convection flow from a vertical cylinder using an equation of state approach, J. Mol. Liq. 277 (2019) 434–452, http://dx.doi.org/10.1016/j.molliq.2018.11.165.
[17] A. Hiremath, G.J. Reddy, O.A. Bég, H. Holla, Numerical Investigation on Transient Third-Grade Magnetized Nanofluid Flow and Radiative Convection Heat Transfer from a Stationary/moving Cylinder: Nanomaterial and Nanoparticle Shape Effects, Waves in Random and Complex Media, 2022, pp. 1–30, http://dx.doi.org/10.1080/17455030.2021.2024300.
[18] G.J. Reddy, A. Hiremath, M. Kumar, O.A. Bég, A. Kadir, Unsteady magnetohydrodynamic couple stress fluid flow from a shrinking porous sheet: variational iteration method study, Heat Transfer 51 (2) (2022) 2219–2236, http://dx.doi.org/10.1002/htj.22397.
[19] R. Mehmood, M.K. Nayak, N.S. Akbar, O.D. Makinde, Effects of thermal-diffusion and diffusion-thermo on oblique stagnation point flow of couple stress Casson fluid over a stretched horizontal Riga plate with higher order chemical reaction, J. Nanofluids 8 (1) (2019) 94–102, http://dx.doi.org/10.1166/jon.2019.1560.
[20] A. Atangana, D. Baleanu, New fractional derivatives with nonlocal and non-singular kernel: theory and application to heat transfer model, arXiv preprint arXiv: 1602 (2016), http://dx.doi.org/10.48550/arXiv.1602.03408. *03408*.
[21] M. Arif, F. Ali, N.A. Sheikh, I. Khan, K.S. Nisar, Fractional model of couple stress fluid for generalized Couette flow: a comparative analysis of Atangana–Baleanu and Caputo–Fabrizio fractional derivatives, IEEE Access 7 (2019) 88643–88655, http://dx.doi.org/10.1109/ACCESS.2019.2925699.
[22] M. Arif, P. Kumam, W. Kumam, I. Khan, M. Ramzan, A fractional model of Casson fluid with ramped wall temperature: engineering applications of engine oil, Comput. Math. Methods (2021) e1162, http://dx.doi.org/10.1002/cmm4.1162.
[23] D. Baleanu, R.P. Agarwal, Fractional calculus in the sky, Adv. Differ. Equ. (1) (2021) 1–9, http://dx.doi.org/10.1186/s13662-021-03454-1.
[24] D. Baleanu, Generalized memory and fractional calculus: a point of view, in: 9th (Online) International Conference on Applied Analysis and Mathematical Modeling, ICAAMM21) June 11-13, Istanbul-Turkey, 2021, p. 92 (Conference Paper).
[25] E. Bas, R. Ozarslan, Real world applications of fractional models by Atangana–Baleanu fractional derivative, Chaos, Solit. Fractals 116 (2018) 121–125, http://dx.doi.org/10.1016/j.chaos.2018.09.019.

[26] M.I. Syam, M. Al-Refai, Fractional differential equations with Atangana–Baleanu fractional derivative: analysis and applications, Chaos, Solit. Fractals X 2 (2019), 100013, http://dx.doi.org/10.1016/j.csfx.2019.100013.
[27] T.L. Bergman, F.P. Incropera, D.P. DeWitt, A.S. Lavine, Fundamentals of Heat and Mass Transfer, John Wiley & Sons, 2011 (Book Chapter).
[28] M. Arif, F. Ali, F.N.A. Sheikh, I. Khan, Enhanced heat transfer in working fluids using nanoparticles with ramped wall temperature: applications in engine oil, Adv. Mech. Eng. 11 (11) (2019), 1687814019880987, http://dx.doi.org/10.1177/1687814019880987.
[29] C.P. Kothandaraman, *Heat And Mass Transfer Data Book*. New Age International, 2004 (Book chapter).
[30] S. Khan, M.M. Selim, A. Khan, A. Ullah, T. Abdeljawad, M. Ayaz, W.K. Mashwani, On the analysis of the non-Newtonian fluid flow past a stretching/shrinking permeable surface with heat and mass transfer, Coatings 11 (5) (2021) 566, http://dx.doi.org/10.3390/coatings11050566.
[31] A. Fabich, *High Power Proton Beam Shocks and Magnetohydrodynamics in a Mercury Jet Target for a Neutrino Factory* (Doctoral Dissertation, Tech. U. Wienna), 2002 (Thesis).
[32] M. Asadullah, U. Khan, R. Manzoor, N. Ahmed, S.T. Mohyud-Din, MHD flow of a Jeffery fluid in converging and diverging channels, Int. J. Mod. Math. Sci 6 (2) (2013) 92–106 (Article in Modern Scientific press).
[33] F. Ali, M. Arif, I. Khan, N.A. Sheikh, M. Saqib, Natural convection in polyethylene glycol based molybdenum disulfide nanofluid with thermal radiation, chemical reaction and ramped wall temperature, Int. J. Heat Technol. 36 (2) (2018) 619–631. http://hdl.handle.net/10453/133891.
[34] L. Zheng, Y. Liu, X. Zhang, Slip effects on MHD flow of a generalized Oldroyd-B fluid with fractional derivative, Nonlinear Anal. R. World Appl. 13 (2) (2012) 513–523, http://dx.doi.org/10.1016/j.nonrwa.2011.02.016.
[35] F.M. Abbasi, M. Gul, I. Shanakhat, H.J. Anjum, S.A. Shehzad, Entropy generation analysis for magnetized peristaltic movement of nanofluid through a non-uniform asymmetric channel with variable thermal conductivity, Chin. J. Phys. 78 (2022) 111–131, http://dx.doi.org/10.1016/j.cjph.2022.05.006.
[36] C.S. Sravanthi, F. Mabood, S.G. Nabi, S.A. Shehzad, Heterogeneous and homogeneous reactive flow of magnetite-water nanofluid over a magnetized moving plate, Propul. Power Res. 11 (2) (2022) 265–275, http://dx.doi.org/10.1016/j.jppr.2022.02.006.
[37] F.M. Abbasi, S.A. Shehzad, Magnetized peristaltic transportation of boron-nitride and ethylene-glycol nanofluid through a curved channel, Chem. Phys. Lett. 803 (2022), 139860, http://dx.doi.org/10.1016/j.cplett.2022.139860.
[38] M. Rashid, S. Nadeem, Flow of EMHD nanofluid in curved channel through corrugated walls, Appl. Math.-A J. Chinese Univ. 37 (4) (2022) 513–529, http://dx.doi.org/10.1007/s11766-022-3899-6.
[39] A. Riaz, S. Almutairi, S.E. Alhazmi, A. Saleem, S. Nadeem, A. Abdelrahman, Insight into the cilia motion of electrically conducting Cu-blood nanofluid through a uniform curved channel when entropy generation is significant, Alex. Eng. J. 61 (12) (2022) 10613–10630, http://dx.doi.org/10.1016/j.aej.2022.04.011.
[40] S. Nadeem, M. Tumreen, B. Ishtiaq, N. Abbas, Three-dimensional Second-Grade Nanofluid Flow with MHD Effects through a Slandering Stretching Sheet: a Numerical Solution, Waves in Random and Complex Media, 2022, pp. 1–19, http://dx.doi.org/10.1080/17455030.2022.2143928.
[41] N. Muhammad, S. Nadeem, F.D. Zaman, Transmission of thermal energy in a ferromagnetic nanofluid flow, Int. J. Mod. Phys. B 36 (32) (2022), 2250236, http://dx.doi.org/10.1142/S0217979222502368.
[42] S. Nadeem, S. Ahmad, A. Issakhov, I.M. Alarifi, MHD stagnation point flow of nanofluid with SWCNT and MWCNT over a stretching surface driven by Arrhenius kinetics, Appl. Math.-A J. Chinese Univ. 37 (3) (2022) 366–382, http://dx.doi.org/10.1007/s11766-022-3966-z.
[43] K.R. Rajagopal, M. Ruzicka, A.R. Srinivasa, On the Oberbeck-Boussinesq approximation, Math. Model Methods Appl. Sci. 6 (8) (1996) 1157–1167, http://dx.doi.org/10.1142/S0218202596000481.
[44] Y.C. Fung, A First Course in Continuum Mechanics, (Book in Englewood Cliffs), Englewood Cliffs, 1977.
[45] C. Truesdell, W. Noll, C. Truesdell, W. Noll, The Non-linear Field Theories of Mechanics, Springer Berlin Heidelberg, 2004, pp. 1–579, http://dx.doi.org/10.1007/978-3-662-10388-3_1.
[46] R.K. Lodhi, K. Ramesh, Comparative study on electroosmosis modulated flow of MHD viscoelastic fluid in the presence of modified Darcy's law, Chin. J. Phys. 68 (2020) 106–120, http://dx.doi.org/10.1016/j.cjph.2020.09.005.
[47] F. Ali, Z. Ahmad, M. Arif, I. Khan, K.S. Nisar, A time fractional model of generalized Couette flow of couple stress nanofluid with heat and mass transfer: applications in engine oil, IEEE Access 8 (2020) 146944–146966, http://dx.doi.org/10.1109/ACCESS.2020.3013701.
[48] R. Garrappa, M. Popolizio, Evaluation of generalized Mittag–Leffler functions on the real line, Adv. Comput. Math. 39 (1) (2013) 205–225, http://dx.doi.org/10.1007/s10444-012-9274-z.